DOI: 10.1002/chem.201201317

Synthesis, Structure, and Reactivity of Borole-Functionalized Ferrocenes

Holger Braunschweig,*[a] Ching-Wen Chiu,[a] Daniela Gamon,[a] Martin Kaupp,[b] Ivo Krummenacher,[a] Thomas Kupfer,[a] Robert Müller,[b] and Krzysztof Radacki[a]

Abstract: Herein, we report on the synthesis of ferrocenylborole [Fc-$(BC_4Ph_4)_2$] featuring two borole moieties in the 1,1′-positions. The results of NMR and UV/Vis spectroscopy and X-ray diffraction studies provided conclusive evidence for the enhanced Lewis acidity of the boron centers resulting from the conjugation of two borole fragments. This finding was further validated by the reaction of [Fc-$(BC_4Ph_4)_2$] and the 4-Me-NC_5H_4 adduct of monoborole [Fc(BC_4Ph_4)], which led to quantitative transfer of the Lewis base. The coordination chemistry of ferrocenylboroles was further studied by examining their reactivity towards several pyridine bases. Accordingly, the strong Lewis acidity of boroles in general was nicely demonstrated by the reaction of [Fc(BC_4Ph_4)] with 4,4′-bipyridine. Unlike common borane derivatives such as [$FcBMe_2$], which only forms a 2:1 adduct, we also succeeded in the isolation of a 1:1 Lewis acid/base adduct, with one nitrogen donor of 4,4′-bipyridine remaining uncoordinated. In addition, the reduction chemistry of ferrocenylboroles [Fc(BC_4Ph_4)] and [Fc$(BC_4Ph_4)_2$] has been studied in more detail. Thus, depending on the reducing agent and the reaction stoichiometry, chemical reduction of [Fc(BC_4Ph_4)] might lead to the migration of the borolediide fragment towards the iron center, affording dianions with either η^5-coordinated C_5H_4 or η^5-coordinated BC_4Ph_4 moieties. In contrast, no evidence for borole migration was observed during reduction of bisborole [Fc$(BC_4Ph_4)_2$], which readily resulted in the formation of the corresponding tetraanion. Finally, our efforts to further enhance the borole ratio in ferrocenylboroles aiming at the synthesis of [Fc$(BC_4Ph_4)_4$] failed and, instead, generated an uncommon *ansa*-ferrocene containing two borole fragments in the 1,1′-positions and a B_2C_4 *ansa*-bridge.

Keywords: boron · iron · ligand effects · reduction

Introduction

The remarkable linear, nonlinear, and electrooptical properties of boron-containing polymeric materials have stimulated significant interest in this area of research.[1–3] Particularly, systems containing tri-coordinated boron centers have proven their potential for diverse applications such as OLEDs, solar cells, and anion sensing.[1] The vacant p_z orbital at boron is readily accessible, which endows these materials with strong Lewis acidity and promotes efficient electron transport through conjugated systems.[1b,f,4] The electrophilicity also enables the generation and isolation of numerous stable Lewis acid/base adducts with interesting nonlinear optical properties and uncommon reactivity patterns such as photoinduced rearrangement reactions.[5,6] With sterically demanding Lewis bases, frustrated Lewis pairs (FLP) are formed, which have successfully been used in the activation of small molecules such as H_2.[7] In addition to the empty p_z orbital at boron, boroles also feature an antiaromatic 4π electron system, which further enhances the Lewis acidic nature of these species. In fact, boroles rank amongst the most Lewis acidic species known. Even weak donors such as ethers readily coordinate to boroles.[8] This reactivity usually involves dramatic color changes, which makes boroles attractive candidates for sensing applications.[9] Coordination of sterically encumbered bases also offer the opportunity for FLP formation.[9] In general, boroles represent highly colored species, a property that is closely related to their rather small HOMO–LUMO gap. It was nicely demonstrated that careful adjustment of the electronic properties of the *exo*-boron substituent provides easy access to a broad range of colors.[9] Numerous recently published articles have highlighted the unique chemistry of antiaromatic borole systems.[9,10] Their strong Lewis acidity enabled the metal-free activation of H_2 without requiring additives such as weakly coordinating Lewis bases (cf. FLPs). Thus, Piers' perfluorinated pentaarylborole was shown to be capable of readily breaking the H–H bond, even in the solid state.[10d,11] The intrinsic electron deficiency of boroles also becomes evident in the crystal structure of 1-ferrocenyl-2,3,4,5-tetraphenyl-

[a] Prof. H. Braunschweig, Dr. C.-W. Chiu, Dr. D. Gamon, Dr. I. Krummenacher, Dr. T. Kupfer, Dr. K. Radacki
Institut für Anorganische Chemie
Julius-Maximilians Universität Würzburg
Am Hubland, 97074 Würzburg (Germany)
Fax: (+49) 931-31-84623
E-mail: h.braunschweig@uni-wuerzburg.de

[b] Prof. M. Kaupp, Dipl. Chem. R. Müller
Institut für Chemie
Technische Universität Berlin
Straße des 17. Juni 135, 10623 Berlin (Germany)

Supporting information for this article is available on the WWW under http://dx.doi.org/10.1002/chem.201201317.

borole [Fc(BC_4Ph_4)] (**2**; Fc = (η^5-C_5H_5)Fe(η^5-C_5H_4)), which features a direct Fe–B bonding interaction associated with an exceptionally large bending of the borole moiety towards the iron center (dip-angle $\alpha^* = 29.4°$).[9a] Similar interactions have been found for boranes such as [FcBBr_2] (**1**) or the more Lewis acidic annulated borole derivative 9-ferrocenyl-9-bora-fluorene.[12] However, as a consequence of the stronger Lewis acidity of boroles compared with boranes or "annulated" borole derivatives, the Fe–B interaction is much less pronounced in these species, as evidenced by smaller values for the dip-angle (cf. **1**: $\alpha^* = 17.7/18.9°$). It was also demonstrated that an increasing number of boryl substituents at ferrocene significantly reduces the dip angle from $\alpha^* = 17.7/18.9°$ in **1** to $\alpha^* = 9.1°$ in [Fc(BBr_2)$_2$] (**3**), which clearly suggests that two boryl fragments share the electron density of the iron center equally. The energetically low-lying LUMO also facilitates the two-electron reduction of boroles to afford aromatic 6π electron borolediides.[8,13] Recently, we communicated a preliminary study dealing with the reduction chemistry of **2**. In this case, addition of two electrons to the borole system entailed an uncommon reduction-induced migration of the borolediide moiety towards the iron center to afford a dianion with a η^5-coordinated BC_4Ph_4 ring.[10e] We now report on our efforts to enhance the borole ratio in ferrocenylboroles. Although we succeeded in the synthesis of bisborole [Fc(BC_4Ph_4)$_2$] (**4**), all attempts to generate the corresponding tetraborole [Fc(BC_4Ph_4)$_4$] (**19**) failed and, instead, resulted in the formation of the unexpected *ansa*-ferrocene **21**. In addition, we provide detailed information on the coordination and reduction chemistry of monoborole **2** and bisborole **4**.

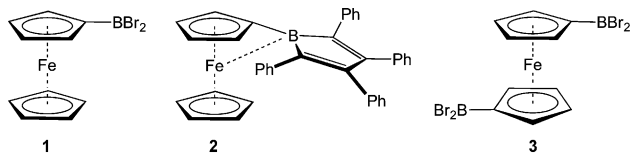

Results and Discussion

Synthesis and characterization of ferrocenyl-1,1′-bis(2,3,4,5-tetraphenylborole) (4): The synthesis of [Fc(BC_4Ph_4)$_2$] (**4**) was readily accomplished by following the well-established boron–tin exchange approach.[8] Thus, reacting [Fc(BBr_2)$_2$] (**3**) with two equivalents of stannole [$Me_2SnC_4Ph_4$] afforded **4** as a reddish brown solid in reasonable isolated yields of 62% (Scheme 1).

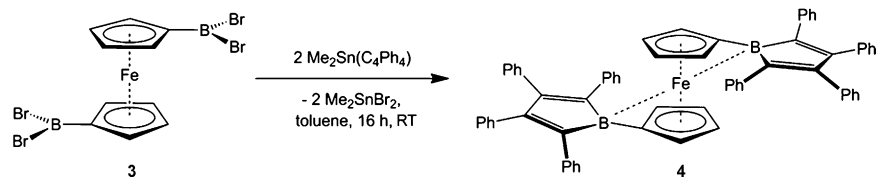

Scheme 1. Synthesis of **4**.

The ^{11}B NMR resonance of **4** ($\delta = 56$ ppm) was detected lowfield-shifted by 6 ppm in comparison to the borane precursor **3**.[14] In contrast, no significant shift was observed during the transformation of **1** ($\delta = 46$ ppm) into the related borole species **2** ($\delta = 46$ ppm).[9] However, it should be kept in mind that, in this case, only a single borole moiety is attached to the ferrocenyl fragment, whereas in **4**, two borole units are capable of interacting with the iron center simultaneously, making them less effective than in **2**. As a result, the ^{11}B NMR signal of **4** appears at lower field than borole **2**. ^{1}H NMR spectroscopic parameters of **4** are unremarkable. Thus, two multiplets are found for the ferrocenyl protons ($\delta = 3.81$–3.82, 4.72–4.73 ppm) and three multiplets for the 40 phenyl protons of the unsaturated backbone ($\delta = 6.85$–6.87, 6.97–7.03, 7.11–7.17 ppm). X-ray diffraction experiments served to clarify the molecular structure of **4** in the solid state. Red single crystals were obtained from hexane diffusion into saturated CH_2Cl_2 solutions of **4**.

As anticipated, the Fe–B interaction in **4** is much less pronounced than in **2** (Figure 1, Table 1), which is nicely demonstrated by the small values for the dip-angles α^* defined

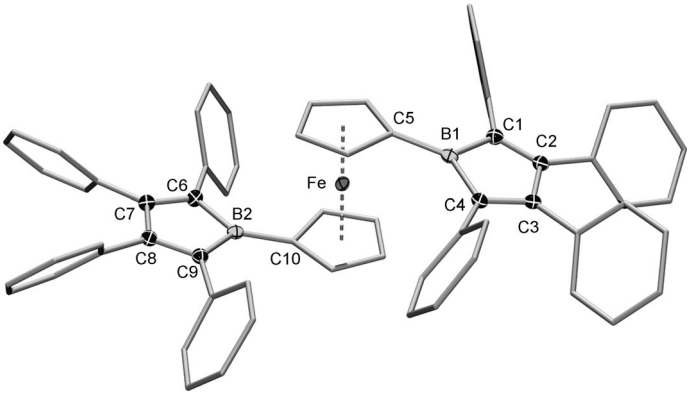

Figure 1. Molecular structure of **4** with thermal ellipsoids set at the 50% probability level. Hydrogen atoms and carbon atoms of the C_5H_4 and phenyl groups are omitted for clarity. Selected bond lengths [Å] and angles [°] are given in Table 1.

by the planes of the C_5H_4 and the respective BC_4 rings. With $\alpha^* = 29.4°$, the dip-angle in **2** is approximately twice as large as those observed for **4** (13.3°, 14.5°).[9a] These findings strongly suggest that the borole moieties of **4** share the electron density from the iron center almost equally in the solid state. Close examination of relevant torsion angles reveals a roughly antiperiplanar arrangement of the borole fragments (B1-C5-C10-B2 160.9°) and a staggered conformation of the ferrocenyl Cp rings (C5-X_{Cp1}-X_{Cp2}-C5′ 17.9°; C10-X_{Cp2}-X_{Cp1}-C10′ 17.8°; X_{Cp} = centroid C_5H_4 ring; Figure 5). In analogy to the borane precursor **3**, which exhibits an ideal anti conformation (ϕ 180°) of the two BBr_2

Table 1. ^{11}B NMR shifts [ppm] and structural parameter of free boroles **2**[9a] and **4**, and their adducts **5**–**7**, **9**, and **10** with bond lengths [Å] and angles [°].

	2	**5**	**6**	**7**[a]	**4**	**9**[a]	**10**
$\delta(^{11})$B	47	1.8	3.2	2.2	56	1.7, 45	1.7
B1,2–C1,6	1.597	1.633(2)	1.630(6)	1.625(3)	1.585(2), 1.582(2)	1.618(5), 1.596(5)	1.623(4), 1.629(4)
B1,2–C4,9	1.582	1.631(2)	1.630(6)	1.620(3)	1.589(2), 1.584(2)	1.633(5), 1.604(5)	1.630(4), 1.637(4)
B1,2–C5,10	1.525	1.602(2)	1.594(6)	1.601(3)	1.518(2), 1.520(3)	1.617(5), 1.499(5)	1.599(4), 1.605(4)
C1,6–C2,7	1.358	1.363(2)	1.344(5)	1.353(3)	1.354(2), 1.351(2)	1.356(5), 1.344(5)	1.353(4), 1.344(4)
C2,7–C3,8	1.518	1.496(2)	1.505(5)	1.498(3)	1.585(2), 1.522(2)	1.495(5), 1.521(5)	1.500(4), 1.506(4)
C3,8–C4,9	1.353	1.356(2)	1.361(5)	1.357(3)	1.356(2), 1.356(2)	1.359(5), 1.351(5)	1.355(4), 1.368(4)
α^*[b]	29.4	0.4	1.5	1.9	14.5, 13.4	1.8, 24.5	2.6, 2.1
β[c]	1.3	48.9	48.7	51.2	3.0, 4.2	49.1, 0.2	50.6, 51.8
B1,2–N1,2	–	1.636(2)	1.651(6)	1.623(3)	–	1,626(5)	1.639(4), 1.633(4)

[a] **7** and **9** contain two independent molecules in the asymmetric unit, which feature similar structural parameters; in both cases, only one molecular structure is discussed; [b] α^*: X_{Cp}-C_{ipso}-B (X_{Cp}: centroid C_5H_4-ring); [c] β: C_{ipso}-B-X_B (X_B: centroid borole ring).

substituents, this arrangement is most likely a direct consequence of the simultaneous interaction of the two Lewis acidic boron nuclei with the metal center of the ferrocenyl fragment. In addition, the borole moieties of **4** show structural features reminiscent of related borole derivatives such as the propeller-like arrangement of the phenyl groups at the butadiene backbone and the almost planar geometry of the BC_4 rings (torsion angles between −2.7(2)° and 2.4(2)°). Similar to **2**, the butadiene backbone features localized single and double bonds, and the boron atom is found in a distorted trigonal-planar environment. The electronic structure of **4** was also assessed by means of UV/Vis spectroscopy; Figure S1 shows a portion of the UV/Vis spectra of **2** and **4** in solution, and the absorption maxima and extinction coefficients are summarized in Table 2. In CH_2Cl_2 solution, the borole chromophore of **2** gives rise to an absorption band at λ_{max} = 398 nm,[9a,10e] whereas the corresponding absorption of **4** was significantly red-shifted by 46 nm (λ_{max} = 444 nm). This finding might be ascribed to the presence of a weaker Fe–B interaction and/or an elongation of the conjugated π system. Interestingly, examination of the spectroscopic parameters of BBr_2- and borole-functionalized ferrocene derivatives reveals a correlation between the UV/Vis maxima and ^{11}B NMR chemical shifts. Thus, a lowfield-shifted ^{11}B NMR signal ($\Delta\delta$ = 4 ppm) and a red-shifted electronic absorption ($\Delta\lambda_{max}$ = 22 nm) are found for boranes **1** and **3**. The corresponding values for borole derivatives **2** and **4** are approximately twice as large ($\Delta\delta$ = 9 ppm; $\Delta\lambda_{max}$ = 46 nm), and a trend of approximately 5 nm per ppm can be derived.

Table 2. Absorption maxima λ_{max} [nm] and extinction coefficients ε [L mol^{-1} cm^{-1}].

Compound	Maxima (extinction coefficients)			
1	461 (995)	343 (3031)	270 (10439)	
2	490 (3791)	398 (3904)	265 (–[a])	
3	483 (1253)	346 (3744)	273 (–[a])	
4	444 (6901)	331 (17956)	266 (–[a])	
5	345 (8853)	260 (–[a])		
6	485 (867)	337 (–[a])		
9	500 (2817)	331 (15602)	261 (–[a])	
10	344 (15101)	259 (46492)		
18	510 (997)	413 (3957)	347 (–[a])	278 (–[a])
21	548 (7857)	458 (7040)	330 (36665)	265 (–[a])

[a] Not available.

Synthesis and characterization of Lewis base adducts of 1-ferrocenyl-2,3,4,5-tetraphenylborole (2): Boroles readily form stable Lewis acid/base adducts with electron donors such as pyridine. Reaction of **2** with equimolar amounts of the pyridine bases 4-R-NC_5H_4 (R = Me, CN) in CH_2Cl_2 was fast and quantitatively afforded the corresponding adducts **5** and **6** (Scheme 2). For **5**, the transformation was accompanied by a characteristic color change from dark-red to yellow, and, after slow evaporation of the solvent, **5** was isolated in 83% yield. Adduct formation was clearly confirmed by the observation of a ^{11}B NMR signal at δ = 1.8 ppm, indicating the presence of a tetracoordinated boron center. ^{1}H NMR spectroscopic data in solution further support the assigned composition of **5**. Thus, a new set of signals is detected for the Cp protons (δ = 3.55, 4.04, 4.10 ppm), whereas the aromatic protons of the BC_4 backbone (δ = 6.60–6.61, 6.94–7.11 ppm) and the Lewis base (δ = 7.42–7.43, 8.67–8.68 ppm) appear as two multiplets each. As expected, the UV/Vis spectrum of **5** features an absorption band at λ_{max} = 345 nm (Figure S2), which is found in the typical region for common borole Lewis acid/base adducts.[9d] In stark contrast to the behavior encountered in the case of **5**, no color change was observed upon addition of 4-CN-NC_5H_4 to a solution of **2**. However, the formation of an adduct was unambiguously verified by ^{11}B NMR spectroscopy, which revealed a sharp singlet for **6** with a chemical shift characteristic for a tetracoordinate boron nucleus (δ = 3.2 ppm). Furthermore, the ^{1}H NMR spectrum of **6** strongly

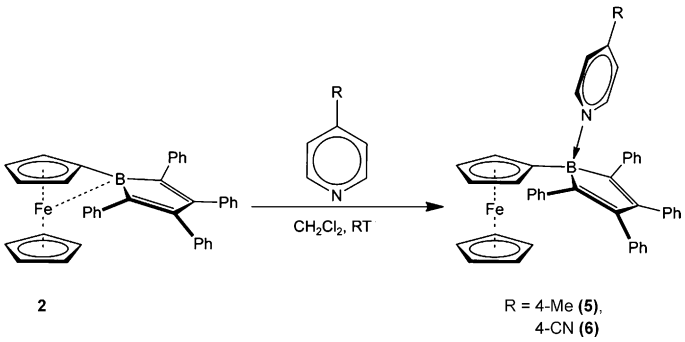

Scheme 2. Lewis acid/base adducts of ferrocenylborole **2**.

resembled that of **5**. Thus, two multiplets for the aromatic pyridine protons are detected that appear slightly shifted to lower field ($\delta = 7.83$–7.84, 9.05–9.06 ppm) with respect to **5**, presumably because of the electron-withdrawing character of the CN substituent. The differing electronic structures of **5** and **6** becomes most evident in the UV/Vis spectrum of **6**, which shows an additional red-shifted absorption at $\lambda_{max} =$ 485 nm. These findings are rather surprising considering the characteristic color changes that are usually observed upon adduct formation.[9b,d] Instead, UV/Vis spectroscopy indicates a comparable electronic absorption behavior of **6** and its borole precursor **2** ($\lambda_{max} = 490$ nm). The presence of Lewis acid/base adducts in the solid state was substantiated for both species by X-ray diffraction (Figure 2). Orange

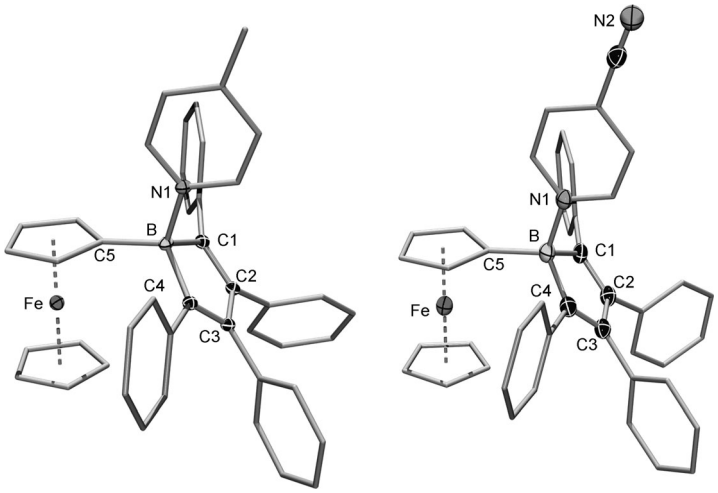

Figure 2. Molecular structures of **5** (left) and **6** (right) with thermal ellipsoids set at the 50% probability level. Hydrogen atoms and carbon atoms at the Cp and phenyl groups are omitted for clarity. Selected bond lengths [Å] and angles [°] are given in Table 1.

single crystals of **5** and dark-red needles of **6** were obtained by slow diffusion of hexane into saturated CH_2Cl_2 solutions. As expected, coordination of 4-Me-NC_5H_4 resulted in the generation of an sp^3-hybridized, electronically saturated boron center in **5**. Consequently, the dip-angle $\alpha^* = 0.3°$ is significantly reduced compared with **2** ($\alpha^* = 29.4°$), which clearly suggests the absence of any Fe–B interaction in the molecular structure of **5**. Electronic saturation of the borole fragment is also highlighted by a characteristic elongation of all B–C bonds in **5** compared to **2** (Table 1). In addition, adduct formation is accompanied by a considerable bending of the borole moiety towards the ferrocenyl unit. The B–N bond in **5** (1.636(2) Å) is slightly elongated compared with other adducts such as $[ClBC_4Ph_4]\cdot(4\text{-Me-}NC_5H_4)$ (1.602(3) Å)[9b] or $[(OC)_3Mn(\eta^5\text{-}C_5H_4BC_4Ph_4)]\cdot(4\text{-R-}NC_5H_4)$ (R = *t*Bu 1.619(3) Å; R = NMe_2 1.608(3) Å).[9d] In contrast, coordination of the Lewis base does not affect the planarity of the BC_4 ring, as evidenced by torsion angles between −3.8(2)° and 3.2(2)°. The structural parameters of **6** are similar to those of **5**. Only the B–N1 bond (1.651(5) Å) is slightly longer, which is most likely a result of the less pronounced Lewis basicity of 4-CN-NC_5H_4 in comparison to 4-Me-NC_5H_4.

Stoichiometric reaction of **2** with 4,4′-bipyridine in CH_2Cl_2 results in the formation of two different types of Lewis acid/base adducts. Whereas **7** represents the anticipated 1:1 adduct, **8** contains the bidentate Lewis base in a bridging position between two molecules of **2** (Scheme 3). Compounds **7** and **8** can readily be separated based on their different solubilities; thus, **7** remains in solution while **8** is much less soluble and precipitates as a red solid during the course of the reaction. In the case of **7**, adduct formation was clearly confirmed by NMR spectroscopy. Again, a sharp resonance in the ^{11}B NMR spectrum ($\delta = 2.2$ ppm) is indicative of a tetracoordinated boron center. Moreover, the presence of four distinct multiplets ($\delta = 7.66$–7.67, 7.87–7.88, 8.83–8.84, 8.96–8.97 ppm) in the ^1H NMR spectrum of **7** for the eight aromatic protons of 4,4′-bipyridine, as well as their relative intensities with respect to the Ph ($\delta = 6.65$–6.67 (4H), 6.97–7.13 ppm (16H)), C_5H_4 ($\delta = 3.61$–3.62 (2H), 4.08–4.09 ppm (2H)), and C_5H_5 protons ($\delta = 4.13$ ppm (5H)) further supports the coordination of only one molecule of **2**. In contrast, the NMR study of **8** proved much more challenging because of its low solubility even in hot benzene, and no ^{11}B NMR signal could be detected. ^1H NMR data of **8** were

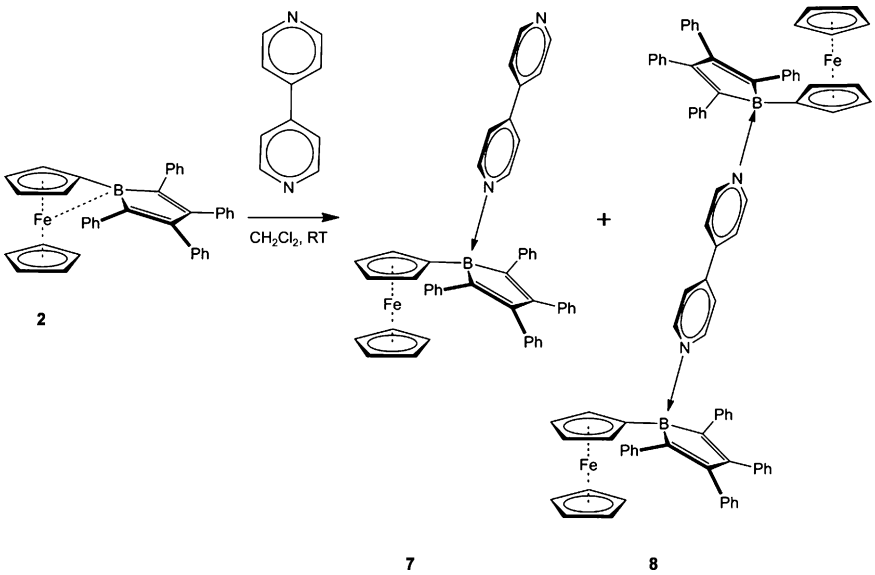

Scheme 3. Synthesis of 4,4′-bipyridine adducts **7** and **8**.

eventually obtained in C_6D_6 at 70 °C. The most notable feature is the presence of only two multiplets for the eight 4,4′-bipyridine protons ($\delta = 6.46$–6.47, 8.95–8.96 ppm) resulting from the higher symmetry of **8** compared with **7**. Integration of all ^{1}H NMR resonances was also in agreement with the formation of a 2:1 adduct. The synthesis of **7** could also be carried out with high selectivity by addition of an excess of 4,4′-bipyridine to a solution of **2**. It should also be noted that related ferrocenylboranes such as [FcBMe$_2$] do not form 1:1 adducts with 4,4′-bipyridine comparable to **7**, and only species with a 2:1 composition have been isolated so far.[15] These findings suggest that the high Lewis acidity of boroles is required to effectively reduce the basicity of the second nitrogen donor site of 4,4′-bipyridine and to preclude additional coordination. The results of an X-ray diffraction study on orange single crystals of **7** finally confirmed the formation of a 1:1 adduct (Figure 3, Table 1).

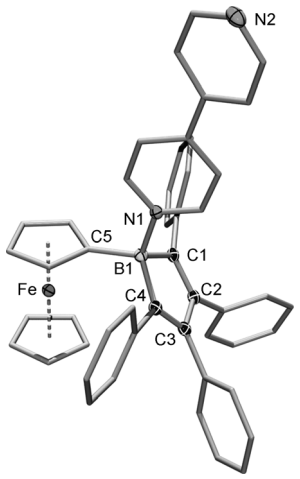

Figure 3. Molecular structure of **7** with thermal ellipsoids set at the 50% probability level. The asymmetric unit contains two independent molecules; only one is shown. Hydrogen atoms and carbon atoms at the Cp and phenyl groups are omitted for clarity. Selected bond lengths [Å] and angles [°] are given in Table 1.

Similar to the solid-state structures of **5** and **6**, the borole moiety in **7** is bent towards the ferrocenyl fragment, whereas the bidentate Lewis base points in the opposite direction. Interestingly, the two pyridine rings of the 4,4′-bipyridyl moiety are not arranged in a coplanar manner, as evidenced by a torsion angle of 25.8/18.2° (two independent molecules in the asymmetric unit). The enhanced Lewis acidity of boroles over simple boranes is nicely illustrated by the considerably shorter B–N1 bonds in **7** (1.623(3)/1.633(3) Å) than those found in [(FcBMe$_2$)-NC$_5$H$_4$-C$_5$H$_4$N-(BMe$_2$Fc)] (1.682(5) Å, 1.689(4) Å).[15a] Unfortunately, no direct comparison with the 4,4′-bipyridine adducts derived from the related borane [FcBMe$_2$] is possible, because 1) the latter only forms the 2:1 adduct [(FcBMe$_2$)-NC$_5$H$_4$-C$_5$H$_4$N-(BMe$_2$Fc)],[15a] and 2) we were not able to obtain structural data on the corresponding borole derivative **8**. Other structural parameters of **7** are unremarkable and similar to those observed for **5** and **6** (Table 1).

Reactivity of 4 towards 4-Me-NC$_5$H$_4$: Isolation and characterization of Lewis acid/base adducts 9 and 10: Coordination of one equivalent 4-Me-NC$_5$H$_4$ to **4** proceeded in a highly selective manner to one single borole center and afforded the 1:1 adduct **9** quantitatively (Scheme 4). Thus, this boron center becomes electronically saturated and is no longer capable of interacting with the iron atom. As a consequence, the Fe–B interaction involving the second borole fragment is significantly strengthened. Evidently, this behavior is responsible for the high selectivity of this transformation, and enables the stepwise synthesis of **9** and the corresponding 2:1 adduct **10** upon coordination of a second molecule of 4-Me-NC$_5$H$_4$. The observation that the color of the reaction mixture remains deep-red after addition of the first equivalent 4-Me-NC$_5$H$_4$ clearly indicates the presence of at least one intact borole system. Conclusive characterization of both species and a stepwise reaction mechanism comes from NMR and UV/Vis spectroscopic experiments in solution. As expected, the ^{11}B NMR spectrum of **9** exhibits two well-separated signals at $\delta = 1.7$ and 45 ppm. Whereas the first resonance is found in the typical region for borole Lewis acid/base adducts featuring a tetracoordinated boron center, the chemical shift of the second signal is indicative of an sp^2-hybridized boron nucleus. In fact, the chemical shift of $\delta =$ 45 ppm strongly resembles that found in the related ferrocenylborole **2** ($\delta = 47$ ppm),[9a] which suggests similar electronic environments and the presence of an intact borole fragment in **9**. In addition, this resonance appears considerably high-field-shifted with respect to the precursor **4** ($\delta = 56$ ppm). Thus, it becomes clear that removal of one Fe–B interaction in **4** by adduct formation notably strengthens the remaining one. Both the integration ratio and the signal pattern of the ^{1}H NMR spectrum of **9** are consistent with the formation of an asymmetric 1:1 adduct. Thus, four multiplets are detected for the C$_5$H$_4$ protons ($\delta = 3.63$, 3.66, 4.29, 4.54 ppm (8H)), whereas the aromatic protons of the Ph groups ($\delta = 6.38$–6.40, 6.90–6.95, 6.99–7.01, 7.11–7.14 ppm (40H)) and the pyridine base ($\delta = 7.35$–7.36, 8.56–8.57 ppm (4H)) give rise to four and two multiplets, respectively. The same conclusions can be extracted from the UV/Vis spectrum of **9** (Figure S3). Coordination of one molecule of 4-Me-NC$_5$H$_4$ to **4** results in the disappearance of the absorption maximum at $\lambda_{max} =$ 444 nm. Instead, the shoulder observed at a wavelength of approximately 500 nm develops into a distinct absorption band at $\lambda_{max} = 500$ nm for **9**. This excitation is thus found in a region similar to that of the related ferrocenylborole **2**, which highlights the close electronic relationship of the latter to the intact borole moiety of **9**. In addition, the intensity of the absorption band at $\lambda_{max} = 331$ nm in **4** decreases and develops into a less well-separated signal for **9**. Similarly, the UV/Vis spectrum of **10** (Figure S3) nicely illustrates the consequences on the electronic properties of the borole fragments within the 2:1 adduct **10** upon coordination of a second molecule of 4-Me-NC$_5$H$_4$.

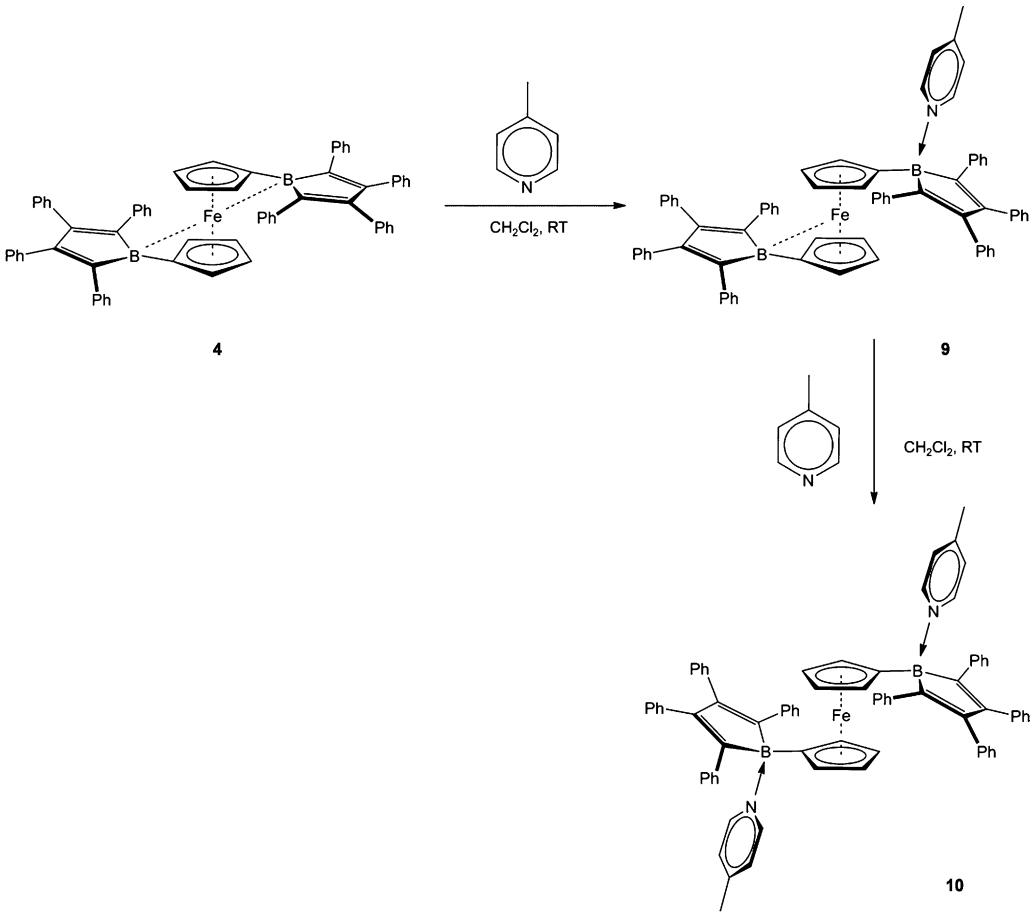

Scheme 4. Coordination of two equivalents of 4-Me-NC_5H_4 to **4**.

Typical of a simple borole Lewis acid/base adduct, only one absorption band is observed at a wavelength of $\lambda_{max}=$ 344 nm, clearly indicating the absence of any conjugated borole system. Because of the higher symmetry of **10** with respect to **9**, the ^{11}B NMR spectrum of **10** features a single resonance for the tetracoordinated boron centers ($\delta=$ 1.7 ppm), and the ^{1}H NMR spectrum shows only two signals for the C_5H_4 protons of the ferrocenyl moiety ($\delta=3.52$, 3.99 ppm). All other NMR spectroscopic parameters are comparable to those of the related species **5**. The molecular structures of **9** and **10** were also studied in the solid state by X-ray diffraction (Figure 4, Table 1). Red (**9**) and orange (**10**) single crystals were grown either by slow diffusion of hexane into saturated CH_2Cl_2 solutions or by slow evaporation of CH_2Cl_2 solutions. Consistent with the results obtained in solution, coordination of one equivalent of the Lewis base 4-Me-NC_5H_4 to **4**, affording the 1:1 adduct **9**, considerably strengthens the Fe–B2 bonding interaction between the iron center and the intact borole fragment, which becomes evident in a much larger dip-angle $\alpha^*=24.5°$ with respect to the precursor **4** (13.3, 14.5°). Thus, the Fe–B interaction in **9** is of similar magnitude to that of **2** ($\alpha^*=29.4°$). Accordingly, adduct formation also precludes any significant electronic communication between the tetracoordinated boron center B1 and iron, which is illustrated by the dip-angle ($\alpha^*=0.2°$). Examination of the B–C bond lengths additionally highlights the different electronic environments of the boron atoms B1 and B2. These differences are most distinct for the B–C_{ipso} bonds, which is noticeably shorter within the intact borole system (cf. B2–C10 1.499(5) Å; B1–C5 1.617(5) Å). The same trend is found for the other B–C bonds, albeit less pronounced (cf. B2–C6 1.596(5) Å; B2–C9 1.604(5) Å; B1–C1 1.618(5) Å; B1–C4 1.633(5) Å). Similar observations have already been made for ferrocenyl borole **2** and its corresponding adduct **5**, and are related to the strong Lewis acidity of the free borole moiety. As indicated by the top view of the molecular structures of bisborole **4** and its adducts **9** and **10**, the torsion angle B1-C5-C10-B2 is significantly reduced from 161° in **4** to 153° in **9**, and finally 123° in **10**. Concomitantly, the torsion of the Cp rings becomes smaller (Figure 5) (cf. 17° for **4**, 8° for **9**, and 5° for **10**). We suggest that coordination of the first equivalent of 4-Me-NC_5H_4 most likely reduces the electronic communication between the two borole fragments in **9**, which becomes even more pronounced after coordination of the second Lewis base and formation of the 2:1 adduct **10**. In addition, this transformation is accompanied by the successive disappearance of any Fe–B bonding interaction. Both factors pre-

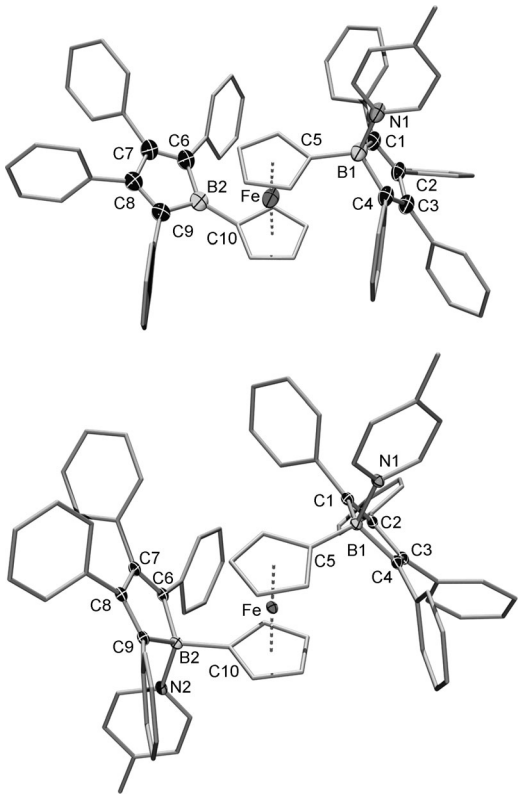

Figure 4. Molecular structures of **9** (top) and **10** (bottom) with thermal ellipsoids set at the 50% probability level. The asymmetric unit of **9** contains two independent molecules; only one is show. Hydrogen atoms and carbon atoms at the Cp and phenyl groups are omitted for clarity. Selected bond lengths [Å] and angles [°] are given in Table 1.

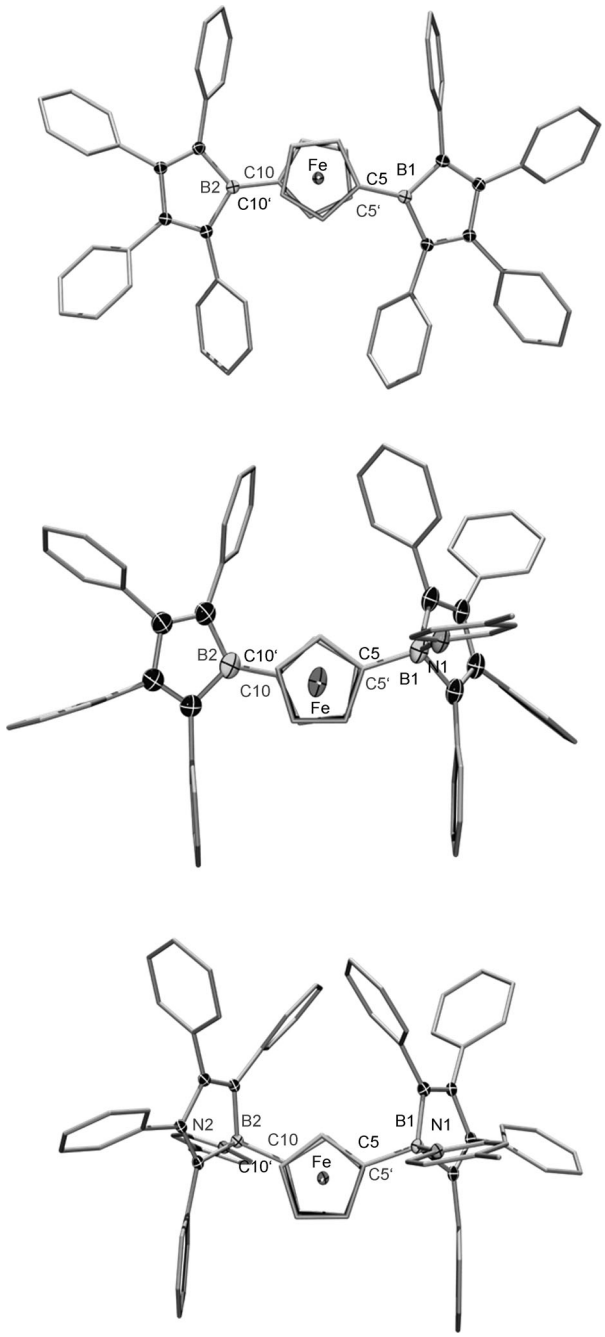

Figure 5. Top view of the molecular structures of **4** (top), **9** (middle), and **10** (bottom).

sumably favor an eclipsed conformation of the ferrocenyl moiety, which was also observed in the monoborole derivatives **2**, **5**, **6**, and **7**.

To further demonstrate the enhanced Lewis acidity of **4** compared with **2**, we performed a base transfer experiment employing the 4-Me-NC_5H_4 adduct **5** and bisborole **4** (Scheme 5). Accordingly, addition of one equivalent of **4** to an orange solution of **5** in CD_2Cl_2 immediately produced the characteristic dark-red color of **2** and **9**. ^{1}H NMR spectroscopic analysis of the reaction mixture clearly confirmed the quantitative transfer of the Lewis base 4-Me-NC_5H_4 from the less Lewis acidic **2** to the more electron-deficient **4**, resulting in the formation of dark-red **9**. In addition, the ^{11}B NMR spectrum features two signals at $\delta = 2$ and 48 ppm, which is consistent with the formation of **2** and **9**, respectively. It should be noted that the lowfield signal is rather broad due to the overlap of the ^{11}B NMR resonances of **2** and the intact borole moiety of **9**. Thus, as anticipated, connecting two borole fragments by a conjugated spacer significantly enhances the Lewis acidity of the system.

Reduction chemistry of 1-ferrocenyl-2,3,4,5-tetraphenylborole 2: We recently communicated on the unique reduction-induced migration of the borole moiety in ferrocenylborole **2** to afford the borole dianion **15**, featuring a η^5-coordinated borole ring.[10e] Whereas in this case excess KC_8 was used as reducing agent, we became more interested in the mechanistic aspects of this remarkable transformation and its dependency on the chosen reductant. To this end, we reinvestigated the reduction of **2** by applying lithium and magnesium metal, as well as magnesium anthracene and solutions of sodium naphthalenide as reducing agents (Scheme 6).

As indicated by a ^{11}B NMR signal at $\delta = 6.8$ ppm, reduction of **2** by excess lithium metal in tetrahydrofuran (THF) resulted in the same migration process already observed for

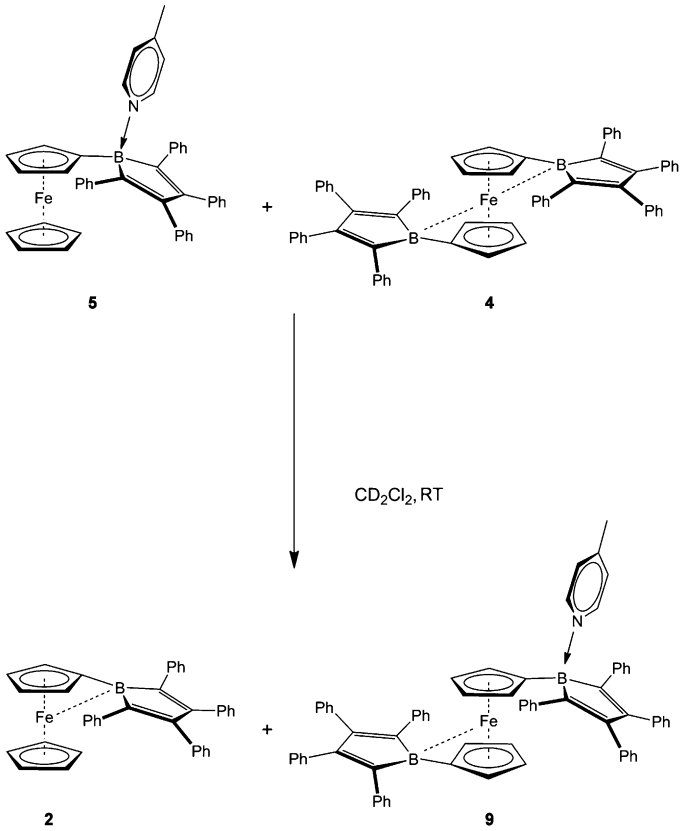

Scheme 5. Base transfer experiment between **5** and bisborole **4**.

the potassium dianion **15**. Further evidence for the presence of a η^5-bound borole ring was provided by the fact that common borole dianions such as $K_2[PhBC_4Ph_4]$ usually show ^{11}B NMR signals with a chemical shift of approximately $\delta = 26$ ppm.[13b] Thus, the appearance of the ^{11}B NMR resonance at much higher field for both **11** and **15** ($\delta = 11$ ppm) appears to be highly indicative of the reduction-induced migration of the borole moiety towards the iron center. Subsequent experiments using sodium naphthalenide as reductant revealed a strong dependence of the migration process on the reaction stoichiometry. The selective formation of **14** is clearly confirmed by its characteristic NMR spectroscopic parameters (^{11}B NMR: $\delta = 23$ ppm; ^1H NMR: $\delta = 3.53$–3.56, 3.63–3.64 ppm). The electronic structure of borole dianions **11**–**15** was also studied by UV/Vis spectroscopy, which revealed a distinct correlation of the lowest-energy excitation of **11**–**15** to the size of the counter cation; a smaller cation leads to a more blue-shifted absorption band (Table 3, Figure S5). Thus, the lowest-energy absorption of **15** is observed at $\lambda_{max} = 489$ nm, whereas the corresponding absorption maxima of **12** and **13**, which contain the much smaller sodium cation, appear at wavelengths of $\lambda_{max} = 459$ and 458 nm, respectively. These results also suggest that migration of the borolediide moiety exerts no significant influence on the energy of the first electronic UV/Vis excitation. Further reducing the size of the cation by employing magnesium leads to an even more blue-shifted absorption band at $\lambda_{max} = 436$ nm. Due to the similar size of the lithium cation,[16] the respective absorption of **11** is expected to fall in the same region as that of **14**. However, this band is not resolved very well, and **11** features only a broad red-shifted shoulder at $\lambda_{max} = 455$ nm in its UV/Vis spectrum. Examination of the borole dianions **11**–**14** by X-ray diffraction eventually substantiated the main structural features derived from the spectroscopic studies in solution (Figure 6 and 7, Table 4). Single crystals of **11**–**14** were obtained by slow evaporation of concentrated THF solutions.

Table 3. Absorption maxima λ_{max} [nm].

11	**12**	**13**	**14**	**15**[10e]
455[a]	459, 370	458, 353,[a] 323	436, 337	489, 388

[a] Absorption represents a poorly resolved shoulder.

As expected, the crystal structure of **11** clearly confirms the migration of the borole moiety to the iron center upon reduction. However, significant differences are found with respect to the molecular structure of **15**. Although both species represent cation-bridged dimers in the solid state, the lithium cation in **11** resides on top of the borolediide moiety. In contrast, the K^+ cations of **15** are exclusively η^5-coordinated to the cyclopentadienyl rings, which is most likely a result of the different ionic radii. Steric repulsion by the bulky BC_4 framework clearly precludes an effective coordination of the large K^+ cation to the borole fragment, whereas the smaller lithium fits perfectly into this pocket. These findings are further illustrated by the considerably

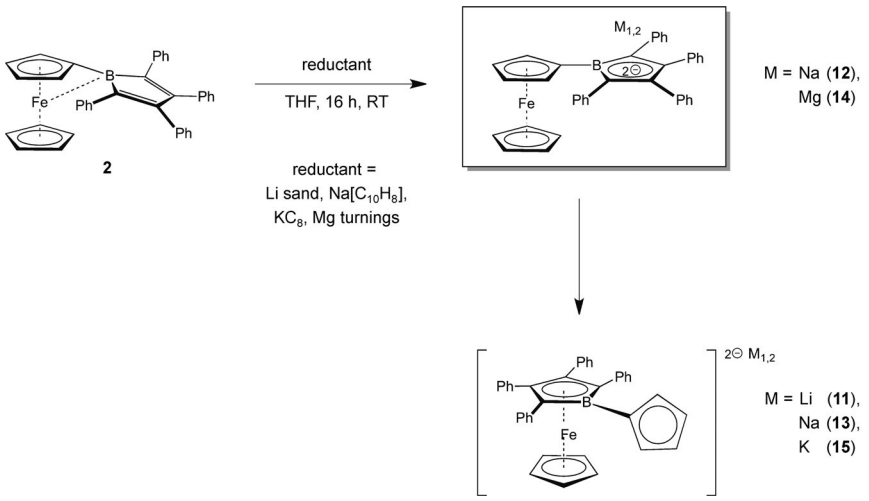

Scheme 6. Reduction chemistry of ferrocenylborole **2**.

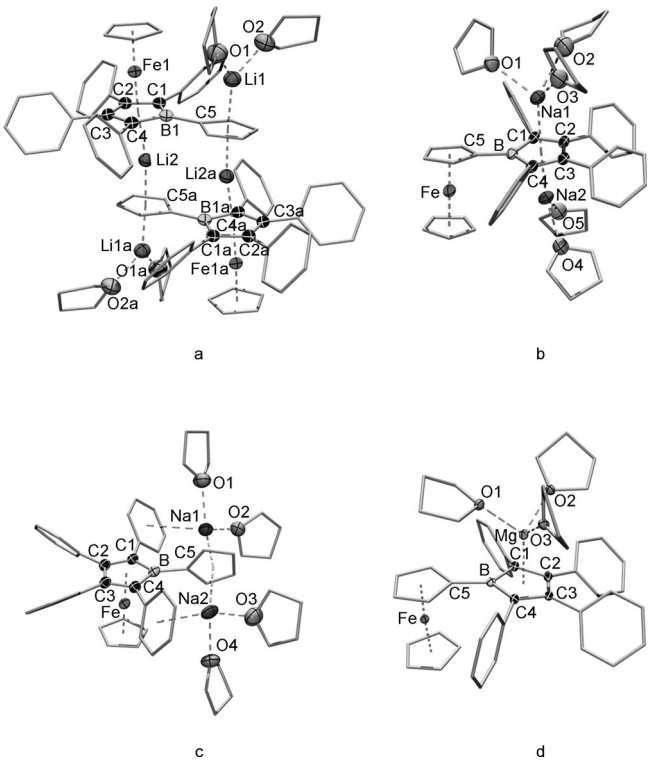

Figure 6. Molecular structures of a) **11**, b) **12**, c) **13**, and d) **14** with thermal ellipsoids set at the 50% probability level. The asymmetric unit of **11** contains two independent molecules; only one is show. **11** is shown as its dimer. Hydrogen atoms and carbon atoms at the Cp and phenyl groups are omitted for clarity. Selected bond lengths [Å] and angles [°] are given in Table 4.

Table 4. ^{11}B NMR shifts [ppm] and structural parameter of **11–16** with bond lengths [Å] and angles [°].

	11[a]	**12**	**13**	**14**	**15**[10e]	**16**
$\delta(^{11}B)$	6.8	20	10	23	12	20
B1(a)–C1(a)	1.563(5)	1.531(4)	1.540(4)	1.538(3)	1.553(4)	1.544(5)
B1(a)–C4(a)	1.551(5)	1.526(4)	1.535(4)	1.536(3)	1.537(4)	1.538(5)
B1(a)–C5(a)	1.581(5)	1.584(4)	1.571(4)	1.576(3)	1.581(4)	1.570(5)
C1(a)–C2(a)	1.464(5)	1.455(4)	1.443(4)	1.455(3)	1.448(4)	1.457(5)
C2(a)–C3(a)	1.445(5)	1.438(4)	1.458(4)	1.430(3)	1.440(4)	1.435(5)
C3(a)–C4(a)	1.459(5)	1.450(4)	1.447(4)	1.453(3)	1.455(4)	1.443(5)
$M_{1,2}$–$X_{B,Cp}$[b]	2.086, 1.985, 1.909	2.460, 2.348	2.403, 2.475	2.068	2.744, 3.025	1.931, 1.780
γ[c]	4.6	13.1	73.0	8.6	60.0	8.0

[a] Compound **11** contains two independent molecules in the asymmetric unit, which feature similar structural parameters; only one molecular structure is discussed; [b] X_B: centroid borole-ring; X_{Cp}: centroid C_5H_4-ring; [c] γ: torsion C_5H_4 plane vs. BC_4 plane.

shorter distances between the metal center and the different five-membered ring systems in **11** (X_B–Li 2.086 Å; Li–X_{C5H4} 1.985/1.909 Å; X_B = centroid borole ring; $X_{C5H4/5}$ = centroids C_5H_4 and C_5H_5 rings) compared with **15** (K1–X_{C5H4} 2.744 Å; X_{C5H4}–K2 2.750 Å; K2–X_{C5H5} 3.025 Å). Another noticeable difference between the molecular structures of **11** and **15** is given by the magnitude of the torsion between the borole unit and the respective C_5H_4 ring, which is only weakly evident in **11** (4.6°) in comparison with **15** (60°). Unlike **11** and **15**, dianions **12** and **13** do not form dimers in the solid state. In addition, X-ray diffraction unambiguously confirmed that no rearrangement was involved during the synthesis of **12**, whereas borole migration clearly occurred for **13**. The two Na^+ cations of **12** are found above and below the plane defined by the borole dianion and both feature a η^5 coordination mode. As expected on the basis of cation size, the Na-centroid distances (Na1–X_B 2.460 Å; Na2–X_B 2.348 Å) lie between those observed in **11** and **15**. The sodium cations are further stabilized by the coordination of two and three THF solvent molecules, respectively. In addition, the angle between the planes of the borole and the C_5H_4 rings is rather small (12°), which is related to the steric requirements of the bulky BC_4 backbone; further torsion would result in steric repulsion by the ferrocenyl moiety. In contrast, the molecular structure of **13** features a very large twist of the C_5H_4 ring with respect to the borole moiety (73.0°), which is easily rationalized given the substantially different connectivities of both species. In **13**, it is the borolediide system that is coordinated to the iron center, and the rather small C_5H_4 substituent can easily rotate out of the BC_4 plane without encountering any significant steric repulsion. Another reason for the pronounced torsion of the C_5H_4 plane is provided by the fact that the singly negatively charged Cp ring in **13** must accommodate two positive charges of the sodium cations, which is achieved by the additional coordination of both Na^+ centers to one phenyl group of the borole backbone.

Thus, the two negative charges of the borolediide systems are not centered within the BC_4 ring, but are most likely delocalized over the whole borole moiety. Coordination of two THF molecules serves to complete the coordination sphere of the Na^+ cations. Finally, the molecular structure of dianion **14** confirms the presence of common ferrocenyl and borolediide fragments and strongly resembles that of **12**. Accordingly, no significant twist of the borole moiety with respect to the η^5-bound C_5H_4 plane is observed (8.6°). The Mg^{2+} cation resides above the BC_4 plane and is further coordinated by three THF molecules. A reasonable explanation for the missing tendency of **2** for borole migration upon reduction by magnesium-based reductants is most likely related to the small ionic radius of Mg^{2+}, and to its doubly charged nature. As a consequence, the small Mg^{2+} cation is able to approach the BC_4 ring system without difficulty (Mg–X_B 2.068 Å), whereas the electrostatic interaction is much stronger than that emerging from singly charged alkaline metals (Figure 7). Common structural features of borole dianions **11–15** in comparison to the precursor **2** are 1) less alternating bond lengths within the BC_4 ring, (ii) elongated B–C_{ipso} bonds, and (iii) shorter B–C bonds within the BC_4 system.

Reduction chemistry of bisborole 4: As a logical development of the results presented above, we also became inter-

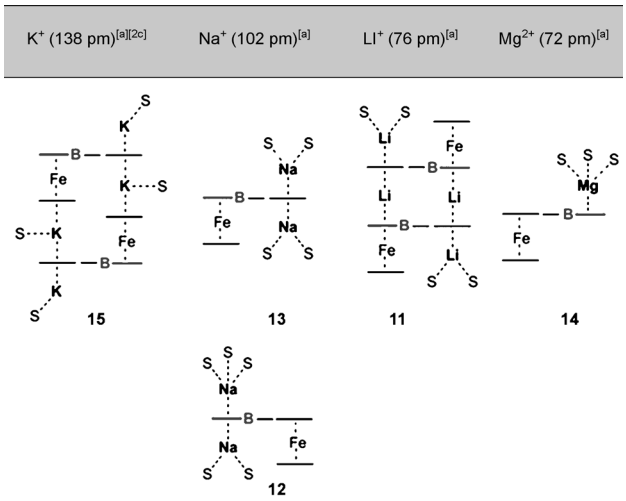

Figure 7. Schematic drawing of the structural motifs found in the solid-state structures of **11**–**15**[10e] (S = THF; [a] = Ionic radius).

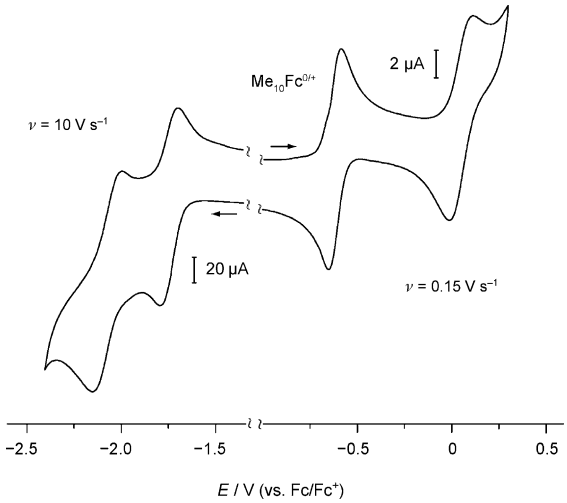

Figure 8. Cyclic voltammetry of **4** at room temperature in CH_2Cl_2 (0.1 M $[Bu_4N][BAr^f_4]$). Scan rate 10 Vs^{-1} (reduction), 150 mVs^{-1} (oxidation). The potential scale is relative to the Fc/Fc^+ couple.

ested in the electrochemistry of bisborole **4**. Initially, the redox behavior of **4** was studied with cyclic voltammetry in CH_2Cl_2 (0.1 M $[NBu_4][BAr^f_4]$; potential referenced against the Fc/Fc^+ couple; Figure 8). Electrochemical experiments were performed in a glove box due to the high reactivity of **4** towards air and moisture. The first reduction event of **4** occurs reversibly at $E_{1/2} = -1.78$ V and, thus, at a more positive potential than for the related ferrocenylborole **2** ($E_{1/2} = -1.95$ V), which highlights again the stronger electron deficiency of two conjugated borole moieties. A second reduction wave was observed relatively close to the first at a potential of $E_{1/2} = -2.11$ V. In contrast to the quasireversible and irreversible nature of the first and second reduction process of **2** ($E_{1/2} = -1.95$ and -2.52 V), both reductions were found to be reversible for bisborole **4** at very high scan rates of 10 Vs^{-1}. The proximity and reversibility of both processes strongly suggest that they are related to the reduction of **4** to afford the monoanion and the diradical-dianion. Further reduction up to the tetraanion is not observed in the cyclic voltammogram of **4**, which, however, might be a consequence of limitations of the solvent potential window. An oxidation at $E_{1/2} = +85$ mV is properly related to the Fe^{II}/Fe^{III} couple. This wave was measured at a much lower scan rate of 150 mVs^{-1} and was found to be reversible.

Chemical reduction of **4** was carried out in THF solution using either lithium or sodium naphthalenide as reductant. Thus, reaction of **4** with excess lithium naphthalenide readily yielded tetraanion **16** as a yellow crystalline material (Scheme 7). It should be mentioned here that the ^{11}B NMR spectrum of **4** in THF features a single resonance at $\delta = 27$ ppm, which is significantly highfield-shifted with respect to the respective signal observed in CH_2Cl_2 solution ($\delta = 56$ ppm) due to a weak interaction between the electron-deficient boron centers and the ethereal oxygen. Reduction to the bis(borolediide) species **16** is clearly indicated by its ^{11}B NMR signal at $\delta = 20$ ppm, which appears in a similar region to those typically found for common borole dianion systems such as **12**, **14**, and $K_2[PhBC_4Ph_4]$ ($\delta = 26$ ppm).[13] Accordingly, ^{11}B NMR spectroscopy strongly suggests that no rearrangement of the borole moiety took place during the reduction process. Further support for the selective formation of a classical borole dianion comes from the ^1H NMR spectrum of **16**, which features C_5H_4 signals ($\delta = 3.56$–3.57, 3.94 ppm) reminiscent of the presence of an intact ferrocene fragment. Consequently, any migratory process can be ruled out. Reduction of **4** with four equivalents of sodium naphthalenide generated the sodium tetraanion **17** as dark-red crystals. The NMR spectroscopic parameters of **17** are comparable to those of **16**, which implies some kind of structural relationship. Hence, the ^{11}B NMR signal of **17** ($\delta = 21$ ppm) again argues against borole migration towards the iron center. The conclusions drawn from NMR spectroscopy in solution are fully substantiated by X-ray diffraction studies on both **16** and **17** (Figure 9, Table 4). Unfortunately, low quality data preclude any closer discussion of the crystal structure of **17**, although its expected composition could be validated. However, anal-

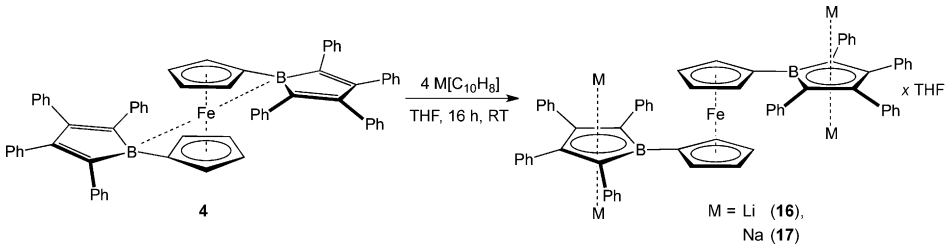

Scheme 7. Synthesis of tetraanions **16** and **17**.

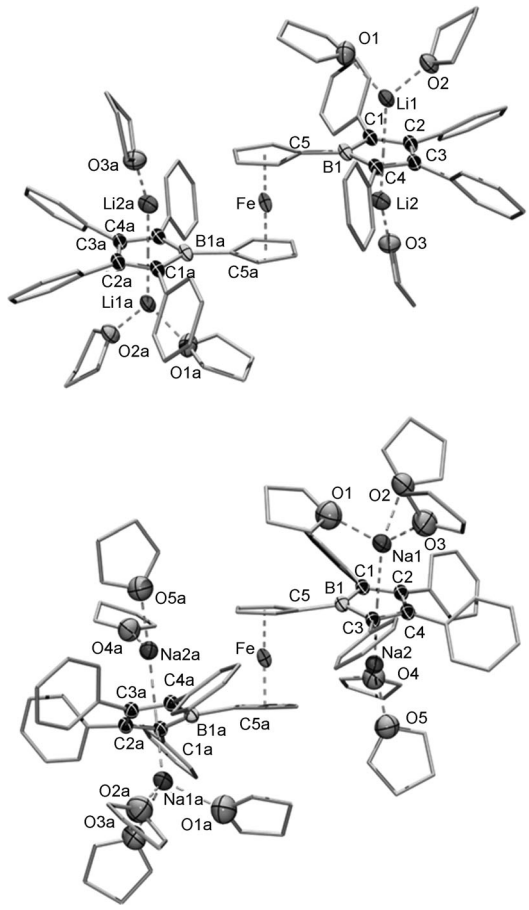

Figure 9. Molecular structures of **16** (top) and **17** (bottom) with thermal ellipsoids set at the 50% probability level. Hydrogen atoms and carbon atoms at the Cp and phenyl groups are omitted for clarity. Selected bond lengths [Å] and angles [°] are given in Table 4.

ysis of the solid-state structure of **16** was possible, which proved that no borole migration occurred during reduction of **4**. The two borole dianion moieties are arranged perfectly antiperiplanar, as evidenced by a torsion angle $\phi = 180°$. Examination of the structural parameters also revealed similarities to the borolediide species **12** and **14**, such as the weakly pronounced twist of the BC_4 ring system with respect to the C_5H_4 plane (8.0°). In addition, the Li^+ cations reside above and below the borolediide ring planes and adopt a η^5 coordination mode. The distances between the lithium centers and the centroids of the BC_4 rings (Li1–X_B 1.931 Å; Li2–X_B 1.780 Å) are even shorter in **16** than in **11**. Similar to the situation in **12**, the Li^+ cations are further stabilized by the coordination of one (Li2) and two (Li1) THF solvent molecules, respectively.

Attempted synthesis of tetraborole 19 and isolation of 1,1′-dibora(dibromotetraphenylbutadien)-3,3′-bis(2,3,4,5-tetraphenylborole)ferrocene (21): To further enhance the borole ratio in ferrocenylboroles, we sought the synthesis of tetraborole **19** by boron–tin exchange reaction of $[Fc(BBr_2)_4]$ (**18**) and $[Me_2SnC_4Ph_4]$ (Scheme 8). After work-up, we were able to isolate a purple solid with a broad ^{11}B NMR signal ($\delta = 63$ ppm) in the region typical of free borole derivatives, which initially prompted us to assume the successful formation of **19**. However, the carbon content of this sample (76.99%) was far too low according to the results of an elemental analysis (**19**: 88.75%). This value rather suggested the presence of a ferrocenylborole containing only three borole moieties and one intact BBr_2 group. With a carbon content of 77.63%, the resulting hypothetical species **20** would match our findings much better. In addition, the MALDI-TOF mass spectrum of the purple solid (*m*/*z* 1454.665) also implied the formation of **20**. However, a closer examination of the ^1H NMR spectrum revealed an ABX spin system for the six ferrocenyl protons, which is not consistent with the anticipated connectivity of **20**. Instead, we rationalized that an *ansa*-type species has formed, in which the two Cp rings are connected over one of their boryl substituents by a tetraphenylbutadiene spacer. Consequently, these results strongly indicated the formation of **21** featuring two borole moieties in 1,1′-positions and an *ansa*-bridge with two -BBr functionalities (Scheme 8). Simulation of the ABX spin system of **21** was in good agreement with the experimental spectrum and helped to provide further support for these assumptions (see the Supporting Information). In addition, the ^{13}C NMR spectrum confirmed the C_2-symmetric nature of **21**, as evidenced by the appearance of five distinct ^{13}C NMR resonances for the ferrocenyl carbon atoms and four signals for the BC_4 borole backbone. Quantum chemical calculations of the ^{13}C NMR spectroscopic parameters enabled partial assignment of the ^{13}C NMR signals (see the Experimental Section and the Supporting Information). Despite the presence of two chemically nonequivalent boron nuclei, the ^{11}B NMR spectrum of **21** features only one resonance at $\delta = 63$ ppm, which is most likely a result of similar chemical shifts for the borole and boryl moieties in combination with the usually observed large half-width of borole ^{11}B NMR signals.

We also studied the electronic properties of **21** by UV/Vis spectroscopy in solution. As expected, the UV/Vis spectrum of **21** shows a rather broad absorption band at $\lambda_{max} = 548$ nm (Figure S4), which appears at a wavelength that is highly characteristic for the lowest-energy excitation of free boroles such as pentaphenylborole ($\lambda_{max} = 560$ nm). Accordingly, no significant Fe–B interaction is present in **21**, which is presumably related to steric repulsion of the bulky borole fragments. We assume that steric congestion is also responsible for the failure to produce the anticipated tetraborole **19**. With respect to reaction mechanism, it appears reasonable that either an open chain mechanism for the formation of the *ansa*-B_2C_4-bridge and **21**, or a reaction sequence consisting of the initial formation of **20** and subsequent comproportionation to afford **21** is involved. Conclusive evidence for the structural composition of **21** was eventually obtained from X-ray crystallography. However, crystallization of **21** consistently yielded only very small needles or very thin plates (0.015×0.09×0.19 mm) of moderate quality. Consequently, the quality of the X-ray diffraction data (RAG

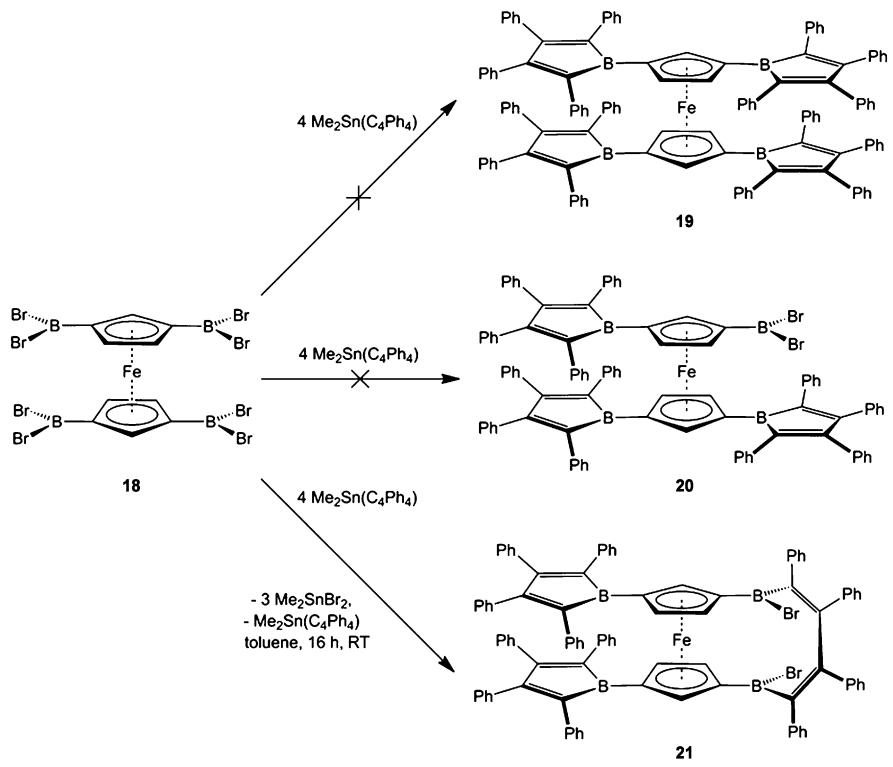

Scheme 8. Attempted synthesis of tetraborole **19**.

2 min/frame; $R1(\sigma > 3\,L) = 12.5\,\%$; $R1(all) = 37.1\,\%$; $R_{int} = 13.0\,\%$; $R_{\sigma} = 59.0\,\%$) was rather low, for which reason a detailed discussion of the structural parameters of **21** is not possible. Nevertheless, the main features of the geometry of **21** in the solid state are clearly validated by this diffraction experiment (Figure 10). All attempts to grow larger crystals of higher quality failed, although numerous solvents, concentrations, and crystallization conditions were tested.

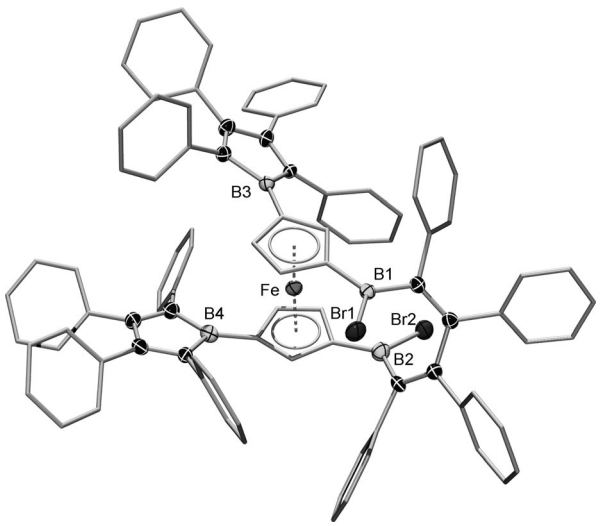

Figure 10. Molecular structure of **21** with thermal ellipsoids set at the 50% probability level. Hydrogen atoms and carbon atoms at the Cp and phenyl groups are omitted for clarity.

Conclusion

This contribution increases our understanding of the chemistry of ferrocenyl-substituted borole derivatives. With the isolation of bisboroles **4** and **21**, we successfully increased the borole ratio in ferrocenylboroles. X-ray crystallography served to confirm the expected 1,1′-structural motif in **4**, and also showed that both borole moieties equally share electron density provided by the iron center through significant Fe–B bonding interactions. In contrast, steric congestion evidently prevented the generation of tetraborole **19** by boron–tin exchange reaction and, instead, led to the formation of the uncommon *ansa*-species **21** containing two borole fragments in 1,1′-positions and an *ansa*-B_2C_4-bridge. The enhanced Lewis acidity of two conjugated borole centers was clearly demonstrated by NMR and UV/Vis spectroscopy, as well as by the reaction of **4** with the pyridine adduct of $[Fc(BC_4Ph_4)]$ (**2**), which resulted in a transfer of the Lewis base to one of the more Lewis acidic boron centers in **4**. Further details on the coordination behavior of ferrocenylboroles **2** and **4** were deduced form their reactivity towards various mono- and bidentate pyridine bases. In the case of **4**, reaction with 4-Me-NC_5H_4 revealed a highly selective and stepwise process to afford the 1:1 and 2:1 adducts **9** and **10**, respectively. Furthermore, these experiments nicely illustrated the strong Lewis acidity of boroles in general, which enabled the isolation of the 1:1 adduct of **2** and the bidentate 4,4′-bipyridine with high selectivity. In addition, the reduction chemistry of ferrocenylboroles **2** and **4** was studied in great detail. Whereas previous results showed that chemical reduction of **2** by excess KC_8 is accompanied by the migration of the borolediide fragment towards the iron center, expansion of this work revealed a strong dependency of the migratory process on the applied reductant and the stoichiometry. In contrast, no evidence for borole migration was found for **4** upon electrochemical reduction or reaction with lithium and sodium naphthalenide, which yielded the tetraanions **16** and **17**, respectively. Thus, ferrocenylboroles show a rich reactivity with both expected and unexpected patterns, and we are confident that borole chemistry will hold many more surprises in the future.

Experimental Section

General conditions: All manipulations were conducted either under an atmosphere of dry argon (5.0) or in vacuo using standard Schlenk line or glove box (MBraun, Innovative Technology) techniques. Solvents were dried according to standard procedures or by using an MBraun solvent purification system and were stored under argon over molecular sieves. C_6D_6, CD_2Cl_2 and [D_8]THF were degassed using three freeze-pump-thaw cycles and stored over molecular sieves. NMR spectra were acquired with a Bruker Avance 500 NMR spectrometer (^{1}H: 500.133 MHz; ^{11}B: 160.364 MHz; ^{13}C: 125.697 MHz). ^{1}H and ^{13}C{^{1}H} NMR spectra were referenced to external TMS by using the residual protons of the solvent (^{1}H) or the solvent itself (^{13}C). ^{11}B NMR spectra were referenced to external $BF_3{\cdot}OEt_2$. UV/Vis spectra were measured with a JASCO V-660 UV/Vis spectrometer. Cyclic voltammetry experiments were conducted in an argon-filled glovebox with a Gamry Instruments Reference 600 potentiostat (C3 Prozess- und Analysentechnik). [$FcBBr_2$] (**1**),[14] [$Fc(BBr_2)_2$] (**3**),[12e] [$Fc(BBr_2)_4$] (**18**),[12e] and [$Fc(BC_4Ph_4)$] (**2**)[9a] were prepared according to literature procedures. 4-Me-NC_5H_4 was dried over CaH_2. Due to their sensitivity towards high vacuum, no elemental analysis could be obtained for **11**–**14**, **16**, or **17**.

Preparation of ferrocenyl-1,1′-bis(2,3,4,5-tetraphenylborole) (4): A solution of **3** (0.50 g, 0.95 mmol) in toluene (4 mL) was treated with [$Me_2SnC_4Ph_4$] (0.96 g, 1.90 mmol) in toluene (6 mL), which was accompanied by a color change from red to dark-reddish-brown. The reaction mixture was stirred for 16 h at ambient temperature. After removal of the solvent, Me_2SnBr_2 was partially removed by sublimation at 40 °C ($3{\cdot}10^{-3}$ mbar) for 1 h. Recrystallization from toluene (4 mL) at −30 °C afforded **4** (0.54 g, 0.59 mmol, 62 %) as a reddish-brown solid, which was washed with hexane (3×3 mL) and dried in vacuo. ^{1}H NMR (CD_2Cl_2): δ = 3.81–3.82 (m, 4H; C_5H_4), 4.72–4.73 (m, 4H; C_5H_4), 6.85–6.87 (m, 8H; C_6H_5), 6.97–7.03 (m, 20H; C_6H_5), 7.11–7.17 ppm (m, 12H; C_6H_5); ^{11}B NMR (CD_2Cl_2): δ = 56 ppm; ^{13}C NMR (CD_2Cl_2): δ = 80.00, 80.26 (CH, C_5H_4), 125.81, 126.91, 127.35, 128.01, 129.34, 129.78 (CH, C_6H_5), 137.61, 141.45, 160.45 (C_q); elemental analysis calcd (%) for $C_{58}H_{48}B_2Fe$: C 86.30, H 5.27; found C 86.11, H 5.36.

Preparation of 1-ferrocenyl[2,3,4,5-tetraphenylborole-1-(4-methylpyridine)] (5): To a solution of **2** (30.0 mg, $5.43{\cdot}10^{-5}$ mol) in CH_2Cl_2 (1 mL) was added 4-Me-NC_5H_4 (5.3 µL, $5.45{\cdot}10^{-5}$ mol), whereupon the color of the solution changed from red to pale-yellow. Slow evaporation of the solvent yielded **5** (29.2 mg, 4.52×10^{-5} mol, 83 %) as orange needles. ^{1}H NMR (CD_2Cl_2): δ = 2.57 (s, 3H; NC_5H_4-4-CH_3), 3.55 (m, 2H; C_5H_4), 4.04 (m, 2H; C_5H_4), 4.10 (s, 5H; C_5H_5), 6.60–6.61 (m, 4H;, C_6H_5), 6.94–7.11 (m, 16H; C_6H_5), 7.42–7.43 (m, 2H; NC_5H_4-4-Me), 8.67–8.68 ppm (m, 2H; NC_5H_4-4-Me); ^{11}B NMR (CD_2Cl_2): δ = 1.8 ppm; ^{13}C NMR (CD_2Cl_2): δ = 21.79 (CH_3, NC_5H_4-4-CH_3), 68.82 (CH, C_5H_5), 69.28, 74.41 (CH, C_5H_4), 124.54, 125.45, 127.01, 127.45, 127.50, 128.73, 130.80 (CH, C_6H_5), 140.74, 144.77 (C_q), 145.51 (CH, NC_5H_4-4-Me), 150.41 (C_q), 154.29 ppm (CH, NC_5H_4-4-Me); elemental analysis calcd (%) for $C_{44}H_{36}BFeN$: C 81.88, H 5.62, N 2.17; found C 80.97, H 5.64, N 2.15.

Preparation of 1-ferrocenyl[2,3,4,5-tetraphenylborole-1-(pyridine-4-carbonitrile)] (6): The synthesis of **6** was carried out in analogy to **5** using **2** (20.0 mg, $3.60{\cdot}10^{-5}$ mol) and 4-CN-NC_5H_4 (3.8 mg, 3.60×10^{-5} mol). Compound **6** (15.2 mg, 2.32×10^{-5} mol, 64 %) was isolated as dark-red needles. ^{1}H NMR (CD_2Cl_2): δ = 3.61 (m, 2H; C_5H_4), 4.10 (m, 2H; C_5H_4), 4.12 (s, 5H; C_5H_5), 6.59–6.61 (m, 4H; C_6H_5), 6.98–7.09 (m, 16H; C_6H_5), 7.83–7.84 (m, 2H; NC_5H_4-4-CN), 9.05–9.06 ppm (m, 2H; NC_5H_4-4-CN); ^{11}B NMR (CD_2Cl_2): δ = 3.2 ppm; ^{13}C NMR (CD_2Cl_2): δ = 68.97 (CH, C_5H_5), 69.85, 74.53 (CH, C_5H_4), 78.33 (C_q, C = C-B), 115.02 (C_q, NC_5H_4-4-CN), 125.01 (CH, C_6H_5 and C_q, NC_5H_4-4-CN), 125.95, 127.57, 127.75, 127.50 (CH, C_6H_5), 128.62 (CH, NC_5H_4-4-CN and C_6H_5), 130.65 (CH, C_6H_5), 140.05, 144.05 (C_q), 151.21 ppm (C_q, C = C-B); elemental analysis calcd (%) for $C_{44}H_{33}BFeN_2$: C 80.51, H 5.07, N 4.27; found C 80.99, H 5.13, N 4.42.

Preparation of 1-ferrocenyl[2,3,4,5-tetraphenylborole-1-(4,4′-bipyridine)] (7) and bis(1-ferrocenyl-2,3,4,5-tetraphenylborole)-1-(4,4′-bipyridine) (8): A solution of **2** (30.0 mg, $5.43{\cdot}10^{-5}$ mol) in CH_2Cl_2 (1 mL) was reacted with 4,4′-bipyridine (8.4 mg, $5.38{\cdot}10^{-5}$ mol). During the addition, the color of the reaction mixture changed from red to orange, and a dark-red precipitate formed. The solid was filtered, washed with hexane, and dried in vacuo to afford **8** (19.2 mg). The solvent of the remaining orange solution was evaporated slowly to yield **7** (5.20 mg) as orange needles, which were washed with hexane and dried in vacuo. ^{1}H NMR (CD_2Cl_2): δ = 3.61–3.62 (m, 2H; C_5H_4), 4.08 (m, 2H; C_5H_4), 4.13 (s, 5H; C_5H_5), 6.65–6.67 (m, 4H; C_6H_5), 6.97–7.13 (m, 16H; C_6H_5), 7.66–7.67 (m, 2H; $C_{10}H_8N_2$), 7.87–7.88 (m, 2H; $C_{10}H_8N_2$), 8.83–8.84 (m, 2H; $C_{10}H_8N_2$), 8.96–8.97 ppm (m, 2H; $C_{10}H_8N_2$); ^{11}B NMR (CD_2Cl_2): δ = 2.2 ppm; ^{13}C NMR (CD_2Cl_2): δ = 68.93 (CH, C_5H_5), 69.55, 74.49 (CH, C_5H_4), 123.94 (CH, $C_{10}H_8N_2$), 124.71, 125.76, 127.56, 127.60 (CH, C_6H_5), 127.72 (CH, $C_{10}H_8N_2$), 128.73, 130.76 (CH, C_6H_5), 140.52, 143.03, 144.57, 145.76 (C_q), 146.83 (CH, $C_{10}H_8N_2$), 150.61 (C_q), 151.50 ppm (CH, $C_{10}H_8N_2$); elemental analysis calcd (%) for $C_{48}H_{37}BFeN_2$: C 81.37, H 5.26, N 3.95; found C 81.68, H 5.52, N 4.31.

Compound 8: ^{1}H NMR (343 K, C_6D_6): δ = 4.18 (m, 4H; C_5H_4), 4.27 (m, 4H; C_5H_4), 4.33 (s, 10H; C_5H_5), 6.46–6.47 (m, 4H; $C_{10}H_8N_2$), 6.93–6.94 (m, 8H; C_6H_5), 6.99–7.06 (m, 24H; C_6H_5), 7.34–7.35 (m, 8H; C_6H_5), 8.95–8.96 ppm (m, 4H; $C_{10}H_8N_2$); elemental analysis calcd (%) for $C_{86}H_{66}N_2B_2Fe$: C 81.93, H 5.28, N 2.22; found C 80.99, H 5.20, N 2.36.

Preparation of ferrocenyl-1-[2,3,4,5-tetraphenylborole-1-(4-methylpyridine)]-1′-(2,3,4,5-tetraphenyborole) (9): 4-Me-NC_5H_4 (4.0 µL, $4.35{\cdot}10^{-5}$ mol) was added to a solution of **4** (40.0 mg, $4.35{\cdot}10^{-5}$ mol) in CD_2Cl_2 (0.6 mL). No color change was observed upon addition. After slow evaporation of the solvent, **9** (39.0 mg, $3.85{\cdot}10^{-5}$ mol, 88 %) was isolated as a red solid. ^{1}H NMR (CD_2Cl_2): δ = 2.56 (s, 6H; NC_5H_4-4-CH_3), 3.63 (m, 2H; C_5H_4), 3.66 (m, 2H; C_5H_4), 4.29 (m, 2H; C_5H_4), 4.54 (m, 2H; C_5H_4), 6.38–6.40 (m, 4H; C_6H_5), 6.90–6.95 (m, 14H; C_6H_5), 6.98–7.01 (m, 12H; C_6H_5), 7.11–7.14 (m, 10H; C_6H_5), 7.35–7.36 (m, 2H; NC_5H_4-4-Me), 8.56–8.57 ppm (m, 2H; NC_5H_4-4-Me); ^{11}B NMR (CD_2Cl_2): δ = 1.7 (B_q), 45 ppm (B_{tr}); ^{13}C NMR (CD_2Cl_2): δ = 21.74 (CH_3, NC_5H_4-4-CH_3), 74.30, 76.81, 78.30, 80.87 (CH, C_6H_5), 124.61, 125.19, 125.63, 126.27 (CH, C_6H_5), 127.06 (CH, NC_5H_4-4-Me), 127.15, 127.35, 127.57, 127.62, 128.49, 129.54, 129.96, 130.49 (CH, C_6H_5), 138.55, 140.16, 142.73, 143.73 (C_q), 145.32 (CH, NC_5H_4-4-Me), 150.49, 154.49, 157.59 ppm (C_q); elemental analysis calcd (%) for $C_{72}H_{55}B_2FeN$: C 85.48, H 5.48, N 1.38; found C 85.10, H 5.48, N 0.97.

Preparation of ferrocenyl-1,1′-bis[2,3,4,5-tetraphenylborole-1-(4-methylpyridine)] (10): 4-Me-NC_5H_4 (6.40 µL, $6.58{\cdot}10^{-5}$ mol) was added to a solution of **4** (30.0 mg, $3.27{\cdot}10^{-5}$ mol) in CD_2Cl_2 (1 mL). Addition was accompanied by a color change from dark-red to pale-yellow. Slow evaporation of the solvent yielded **10** (27.3 mg, $2.47{\cdot}10^{-5}$ mol, 76 %) as orange needles. ^{1}H NMR (CD_2Cl_2): δ = 2.55 (s, 6H; NC_5H_4-4-CH_3), 3.52 (m, 4H; C_5H_4), 3.99 (m, 4H; C_5H_4), 6.53–6.55 (m, 8H; C_6H_5), 6.91–6.93 (m, 12H; C_6H_5), 6.98–7.02 (m, 20H; C_6H_5), 7.34–7.35 (m, 4H; NC_5H_4-4-Me), 8.75–8.76 ppm (m, 4H; NC_5H_4-4-Me); ^{11}B NMR (CD_2Cl_2): δ = 1.7 ppm; ^{13}C NMR (CD_2Cl_2): δ = 21.80 (CH_3, NC_5H_4-4-CH_3), 71.31, 74.15 (CH, C_5H_4), 80.10 (C_q, C = C-B), 124.38, 125.52 (CH, C_6H_5), 126.83 (CH, NC_5H_4-4-Me), 127.38, 127.50, 128.91, 130.82 (CH, C_6H_5), 140.80, 144.73 (C_q), 145.73 (CH, NC_5H_4-4-Me), 154.01, 159.11 ppm (C_q, C = C−B); elemental analysis calcd (%) for $C_{78}H_{62}B_2FeN_2$: C 84.80, H 5.66, N 2.54; found C 83.86, H 5.63, N 2.28.

Preparation of dianion 11: A suspension of lithium sand (5.00 mg, $7.20{\cdot}10^{-4}$ mol) and **2** (0.10 g, $1.81{\cdot}10^{-4}$ mol) in THF (2 mL) was stirred for 16 h at RT. Excess lithium was removed by filtration, and the filtrate was subsequently layered with hexane (40 mL) to afford a dark-red solid. After decanting the liquids, the red precipitate was dissolved in THF (2 mL). Slow evaporation of the solvent yielded yellow crystals of **11**. ^{1}H NMR ([D_8]THF): δ = 1.76 (m, 16H; THF), 3.60 (m, 21H; THF and C_5H_5), 5.81 (m, 2H; C_5H_4), 6.14 (m, 2H; C_5H_4), 6.71 (m, 8H; C_6H_5), 6.81 (m, 4H; C_6H_5), 6.97 (m, 4H; C_6H_5), 7.20 ppm (m, 4H; C_6H_5); ^{11}B NMR ([D_8]THF): δ = 6.8 ppm; ^{13}C NMR ([D_8]THF): δ = 72.23 (CH, C_5H_5), 89.99 (C_q), 103.47, 111.84 (CH, C_5H_4), 121.71, 123.14, 126.03, 126.07, 133.28, 134.03 (CH, C_6H_5), 146.07, 152.40 ppm (C_q).

Preparation of dianion 12: A solution of **2** (0.10 g, $1.81{\cdot}10^{-4}$ mol) in THF (2 mL) was treated with a solution of sodium naphthalenide in THF (1.37 mL, c = 0.28 mol/L, $3.81{\cdot}10^{-4}$ mol). The red reaction mixture was stirred at RT for 16 h and subsequently layered with hexane (40 mL),

which gave a dark-red precipitate. The solution was decanted and the red solid was dissolved in THF (2 mL). Slow evaporation of the solvent yielded dark-red crystals of **12**. ^{1}H NMR ([D$_8$]THF): $\delta = 3.81$ (m, 5H; C$_5H_5$), 3.83 (m, 2H; C$_5H_4$), 4.20 (m, 2H; C$_5H_4$), 6.52–6.55 (m, 4H; C$_6H_5$), 6.69–6.72 (m, 4H; C$_6H_5$), 6.79–6.85 (m, 8H; C$_6H_5$), 7.18–7.20 ppm (m, 4H; C$_6H_5$); ^{11}B NMR ([D$_8$]THF): $\delta = 20$ ppm; ^{13}C NMR ([D$_8$]THF): $\delta = 65.83$ (CH, C_5H$_4$), 67.25 (CH, C_5H$_5$), 71.79 (CH, C_5H$_4$), 117.73, 119.31 (CH, C_6H$_5$), 120.73 (C$_q$), 125.23, 125.39, 131.64, 131.90 (CH, C_6H$_5$), 144.45, 151.10 ppm (C$_q$).

Preparation of dianion 13: Prepared in analogy to **12** employing **2** (0.10 g, $1.81 \cdot 10^{-4}$ mol) and a THF solution of sodium naphthalenide (2.60 mL, $c = 0.28$ mol/L, $7.20 \cdot 10^{-4}$ mol). Compound **13** was isolated as a dark-red solid. ^{1}H NMR ([D$_8$]THF): $\delta = 3.63$ (m, 5H; C$_5H_5$), 5.88–5.89 (m, 2H; C$_5H_4$), 6.36–6.37 (m, 2H; C$_5H_4$), 6.70–6.75 (m, 8H; C$_6H_5$), 6.80–6.83 (m, 4H; C$_6H_5$), 7.01–7.02 (m, 4H; C$_6H_5$), 7.30–7.31 ppm (m, 4H; C$_6H_5$); ^{11}B NMR ([D$_8$]THF): $\delta = 10$ ppm; ^{13}C NMR ([D$_8$]THF): $\delta = 71.19$ (CH, C_5H$_5$), 87.89 (C$_q$), 102.82, 111.95 (CH, C_5H$_4$), 120.62, 122.20, 125.15, 125.33, 131.50, 133.00 (CH, C_6H$_5$), 145.19, 152.43 ppm (C$_q$).

Preparation of dianion 14: A suspension of Mg (9.00 mg, $3.62 \cdot 10^{-4}$ mol) and **2** (0.10 g, $1.81 \cdot 10^{-4}$ mol) in THF (2 mL) was stirred for 16 h at RT. Excess Mg was removed by filtration, and the filtrate was subsequently layered with hexane (40 mL) to afford a dark-red solid. The solution was decanted and the red precipitate was dissolved in THF (2 mL). Slow evaporation of the solvent gave orange crystals of **12**. ^{1}H NMR ([D$_8$]THF): $\delta = 1.72$ (s, 6H; D$_8$-THF), 1.76–1.78 (m, 12H; THF), 3.57 (s, 11H; C$_5H_5$ and D$_8$-THF), 3.60–3.63 (m, 14H; C$_5H_4$ and THF), 3.70–3.71 (m, 2H; C$_5H_4$), 6.56–6.59 (m, 2H; C$_6H_5$), 6.70–6.73 (m, 4H; C$_6H_5$), 6.85–6.88 (m, 2H; C$_6H_5$), 6.98–6.99 (m, 4H; C$_6H_5$), 7.05–7.08 (m, 4H; C$_6H_5$), 7.25–7.27 ppm (m, 4H; C$_6H_5$). ^{11}B NMR ([D$_8$]THF): $\delta = 23$ ppm; ^{13}C NMR ([D$_8$]THF): $\delta = 66.90$, 67.93 (CH, C_5H$_4$), 71.59 (CH, C_5H$_5$), 120.42 (C$_q$), 120.59, 120.99, 125.79, 125.89, 131.74, 132.85 (CH, C$_6$H$_5$), 142.91, 151.45 ppm (C$_q$, C_6H$_5$).

Preparation of tetraanion 16: A solution of **4** (88.0 mg, $9.58 \cdot 10^{-5}$ mol) in THF (2 mL) was reacted with lithium naphthalenide in THF (1.40 mL, $c = 0.30$ mol/L, $4.20 \cdot 10^{-4}$ mol). The red reaction mixture was stirred for 16 h at RT and subsequently layered with hexane (40 mL), which afforded a dark-red precipitate. The solution was decanted and the red solid was dissolved in THF (2 mL). Slow evaporation of the solvent yielded yellow crystals of **16**. ^{1}H NMR ([D$_8$]THF): $\delta = 3.56$–3.57 (m, 4H and 13.5H; C$_5H_4$ and THF), 3.937–3.943 (m, 4H; C$_5H_4$), 6.64–6.67 (m, 4H; C$_6H_5$), 6.72–6.78 (m, 20H; C$_6H_5$), 6.91–6.94 (m, 8H; C$_6H_5$), 7.15–7.16 ppm (m, 8H; C$_6H_5$); ^{11}B NMR ([D$_8$]THF): $\delta = 20$ ppm; ^{13}C NMR ([D$_8$]THF): $\delta = 71.05$, 72.08 (CH, C_5H$_4$), 118.21 (C$_q$), 121.27, 122.27, 126.74, 126.81, 133.05, 133.23 (CH, C_6H$_5$), 142.99, 150.36 ppm (C$_q$).

Preparation of tetraanion 17: A solution of sodium naphthalenide in THF (1.25 mL, $c = 0.28$ mol/L, $3.48 \cdot 10^{-4}$ mol) was added to a solution of **4** (80.0 mg, $8.71 \cdot 10^{-5}$ mol) in THF (2 mL), whereupon the dark-red color of the reaction mixture lightened considerably. After 16 h at ambient temperature, the solution was layered with hexane (40 mL), which resulted in the formation of a dark-red solid. The solution was decanted and the solid was dissolved in THF. Slow evaporation of the solvent yielded **17** as dark-red crystals. ^{1}H NMR ([D$_8$]THF): $\delta = 3.68$–3.69 (m, 4H; C$_5H_4$), 4.12–4.13 (m, 4H; C$_5H_4$), 6.44–6.47 (m, 4H; C$_6H_5$), 6.49–6.52 (m, 4H; C$_6H_5$), 6.65–6.76 (m, 24H; C$_6H_5$), 7.16–7.18 ppm (m, 8H; C$_6H_5$); ^{11}B NMR ([D$_8$]THF): $\delta = 21$ ppm; ^{13}C NMR ([D$_8$]THF): $\delta = 69.76$, 71.89 (CH, C_5H$_4$), 118.17, 120.03 (CH, C_6H$_5$), 121.87 (C$_q$), 126.17, 126.31, 132.76, 133.09 (CH, C_6H$_5$), 145.71, 152.28 ppm (C$_q$).

Preparation of 1,1′-dibora(dibromotetraphenylbutadien)-3,3′-bis[(2,3,4,5-tetraphenyl)borole]ferrocene (21; Figure 11): A solution of **18** (0.43 g, 0.50 mmol) in toluene (4 mL) was treated with [Me$_2$SnC$_4$Ph$_4$] (1.00 g, 2.00 mmol) in toluene (6 mL), which resulted in an immediate color change from red to dark-purple. The reaction mixture was stirred for 16 h at ambient temperature. After removal of the solvent in vacuo, Me$_2$SnBr$_2$ was partially removed by sublimation at 30 °C ($3 \cdot 10^{-3}$ mbar) for 9 h. The residue was dissolved in toluene (4 mL) and stored at −30 °C to afford purple **21** (0.45 g, 0.31 mmol, 62 %), which was washed with hexane (3×3 mL) and dried in vacuo. ^{1}H NMR (CD$_2$Cl$_2$): $\delta = 3.88$–3.89 (t, $J = 1.1$ Hz, 2H; C$_5H_3$), 4.29–4.30 (dd, $J = 1.1$, 2.7 Hz, 2H; C$_5H_3$), 4.36–4.37 (dd, $J = 1.2$, 2.8 Hz, 2H; C$_5H_3$), 6.69–6.70 (m, 4H; C$_6H_5$), 6.74–6.76 (m, 4H; C$_6H_5$), 6.85–6.87 (m, 4H; C$_6H_5$), 6.91–6.93 (m, 6H; C$_6H_5$), 6.99–7.07 (m, 20H; C$_6H_5$), 7.14–7.16 (m, 6H; C$_6H_5$), 7.22–7.24 (m, 12H; C$_6H_5$), 7.31–7.34 ppm (m, 4H; C$_6H_5$); ^{11}B NMR (CD$_2$Cl$_2$): $\delta = 63$ ppm; ^{13}C NMR (CD$_2$Cl$_2$): $\delta = 81.03$ (4-CH, C_5H$_3$), 83.95 (3-C$_q$, C_5H$_3$), 85.57 (1-C$_q$, C_5H$_3$), 86.75 (2-CH, C_5H$_3$), 88.40 (5-CH, C_5H$_3$), 125.95, 126.20, 126.88, 127.09, 127.19, 127.28, 127.32, 127.43, 128.03, 128.44, 128.71, 129.51, 129.70, 129.92, 130.98, 132.72 (CH, C_6H$_5$), 136.79, 136.91 (9,9′-C$_q$), 139.57 (13,12-C$_q$), 140.55 (8,8′-C$_q$), 140.66, 140.97 (6,6′-C$_q$), 141.21 (8,8′-C$_q$), 143.25 (13,12-C$_q$), 148.55 (10-C$_q$), 161.30 (11-C$_q$), 161.78, 162.87 ppm (7,7′-C$_q$); elemental analysis calcd (%) for C$_{94}$H$_{66}$B$_4$FeBr$_2$: C 77.63, H 4.57; found C 76.99, H 4.57; MALDI-TOF-EI-MS: *m*/*z* calcd for C$_{94}$H$_{66}$B$_4$FeBr$_2$: 1454.46; found: 1454.67.

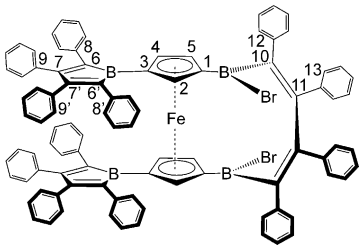

Figure 11. Structure of **21**.

[1] a) C. D. Entwistle, T. B. Marder, *Angew. Chem.* **2002**, *114*, 3051; *Angew. Chem. Int. Ed.* **2002**, *41*, 2927; b) C. D. Entwistle, T. B. Marder, *Chem. Mater.* **2004**, *16*, 4574; c) F. Jäkle, *Coord. Chem. Rev.* **2006**, *250*, 1107; d) M. Elbing, B. C. Bazan, *Angew. Chem.* **2008**, *120*, 846; *Angew. Chem. Int. Ed.* **2008**, *47*, 834; e) A. Lida, S. Yamaguchi, *J. Am. Chem. Soc.* **2011**, *133*, 6952; f) Z. M. Hudson, S. Wang, *Dalton Trans.* **2011**, *40*, 7805.

[2] a) T. Noda, Y. S. Ogawa, Y. Shirota, *Adv. Mater.* **1999**, *11*, 283; b) Y. Shirota, T. Kinoshita, K. Noda, T. O. Okumoto, *J. Am. Chem. Soc.* **2000**, *122*, 11021; c) N. Matsumi, K. Naka, Y. Chujo, *J. Am. Chem. Soc.* **1998**, *120*, 5112; d) H. Li, A. Sundararaman, K. Venkatasubbaiah, F. Jäkle, *J. Am. Chem. Soc.* **2007**, *129*, 5792; e) C.-H. Zhao, A. Wakamiya, J. Inukai, S. Yamaguchi, *J. Am. Chem. Soc.* **2006**, *128*, 15934; f) C. R. Wade, F. P. Gabbai, *Inorg. Chem.* **2010**, *49*, 714; g) C. R. Wade, F. P. Gabbai, *Dalton Trans.* **2009**, 9169.

[3] a) A. Wakamiya, K. Mori, S. Yamaguchi, *Angew. Chem.* **2007**, *119*, 4351; *Angew. Chem. Int. Ed.* **2007**, *46*, 4273; b) J. Qin, G. Cheng, O. Achara, K. Parab, F. Jäkle, *Macromolecules* **2004**, *37*, 7123; c) K. Parab, Y. Quin, F. Jäkle, *Poly. Mater. Sci. Eng. Prepr.* **2005**, *93*, 422; d) M. Häußler, B. Tang, *Adv. Polym. Sci.* **2007**, *209*, 1.

[4] a) W. E. Piers, G. J. Irvine, V. C. Williams, *Eur. J. Inorg. Chem.* **2009**, 2131; b) T. W. Hundall, C.-W. Chiu, F. P. Gabbai, *Acc. Chem. Res.* **2009**, *42*, 388; c) G. Zhou, C.-L. Ho, W.-J. Wong, Q. Wang, D. Ma, L. Wang, Z. Lin, T. B. Marder, A. Beeby, *Adv. Funct. Mater.* **2008**, *18*, 499; d) Z. M. Hudson, S. Wang, *Acc. Chem. Res.* **2009**, *42*, 1584; e) Y. Shirota, *J. Mater. Chem.* **2000**, *10*, 1.

[5] a) H. C. Brown, H. J. Schlesinger, C. Z. Samuel, *J. Am. Chem. Soc.* **2007**, *129*, 7427; b) M. J. G. Lesley, A. Woodward, N. J. Taylor, T. B. Marder, *Chem. Mater.* **1998**, *10*, 1355; c) Z. M. Su, X. J. Wang, R. S. Huang, J. K. Feng, J. K. Sun, *Synth. Met.* **2001**, *119*, 583.

[6] a) Y.-L. Rao, H. Amarne, S.-B. Zhao, T. M. McCornick, S. Martic, Y. Sun, R.-J. Wang, S. Wang, *J. Am. Chem. Soc.* **2008**, *130*, 12898; b) C. Baik, Z. M. Hudson, H. Amarne, S. Wang, *J. Am. Chem. Soc.* **2009**, *131*, 14549; c) H. Amarne, C. Baik, S. K. Murphy, S. Wang, *Chem. Eur. J.* **2010**, *16*, 4750; d) C. Baik, S. K. Murphy, S. Wang, *Angew. Chem.* **2010**, *122*, 8400; *Angew. Chem. Int. Ed.* **2010**, *49*, 8224.

[7] a) S. J. Geier, D. W. Stephan, *J. Am. Chem. Soc.* **2009**, *131*, 3476; b) S. J. Geier, A. L. Gille, D. W. Stephan, *Inorg. Chem.* **2009**, *48*, 10466; c) D. W. Stephan, *Chem. Commun.* **2010**, *46*, 8526.

[8] a) J. J. Eisch, J. E. Galle, S. Kozima, *J. Am. Chem. Soc.* **1986**, *108*, 379; b) J. J. Eisch, N. K. Hota, S. Kozima, *J. Am. Chem. Soc.* **1969**, *91*, 4575.

[9] a) H. Braunschweig, I. Fernandeź, G. Frenking, T. Kupfer, *Angew. Chem.* **2008**, *120*, 1977; *Angew. Chem. Int. Ed.* **2008**, *47*, 1951; b) H. Braunschweig, T. Kupfer, *Chem. Commun.* **2008**, 6427; c) K. Ansorg, H. Braunschweig, C.-W. Chiu, B. Engels, D. Gamon, M. Hügel, T. Kupfer, K. Radacki, *Angew. Chem.* **2011**, *123*, 2937; *Angew. Chem. Int. Ed.* **2011**, *50*, 2885; d) H. Braunschweig, A. Damme, D. Gamon, T. Kupfer, K. Radacki, *Inorg. Chem.* **2011**, *50*, 4250; e) H. Braunschweig, C.-W. Chiu, K. Radacki, T. Kupfer, J. Wahler, *Chem. Eur. J.* **2010**, *16*, 12229; f) H. Braunschweig, C.-W. Chiu, A. Damme, K. Ferkinghoff, K. Radacki, J. Wahler, *Organometallics* **2011**, *30*, 3210.

[10] a) H. Braunschweig, T. Kupfer, *Chem. Commun.* **2011**, *47*, 10903; b) H. Braunschweig, C.-W. Chiu, K. Radacki, P. Brenner, *Chem. Commun.* **2010**, *46*, 916; c) H. Braunschweig, C.-W. Chiu, K. Radacki, T. Kupfer, *Angew. Chem.* **2010**, *122*, 2085; *Angew. Chem. Int. Ed.* **2010**, *49*, 2041; d) H. Braunschweig, C.-W. Chiu, K. Radacki, T. Kupfer, *Inorg. Chem.* **2011**, *50*, 62; e) H. Braunschweig, F. Breher, C.-W. Chiu, D. Gamon, D. Nied, K. Radacki, *Angew. Chem.* **2010**, *122*, 9159; *Angew. Chem. Int. Ed.* **2010**, *49*, 8975; f) J. Köhler, S. Lindenmaier, I. Fischer, H. Braunschweig, T. Kupfer, D. Gamon, C.-W. Chiu, *J. Raman Spectrosc.* **2009**, *41*, 636.

[11] a) C. Fan, W. E. Piers, M. Parvez, *Angew. Chem.* **2009**, *121*, 2999; *Angew. Chem. Int. Ed.* **2009**, *48*, 2955; b) C. Fan, W. E. Piers, M. Parvez, R. McDonald, *Organometallics* **2010**, *29*, 5132; c) C. Fan, L. G. Mercier, H. W. Tuononen, W. E. Piers, M. Parvez, *J. Am. Chem. Soc.* **2010**, *132*, 9604.

[12] a) T. Renk, W. Ruf, W. Siebert, *J. Organomet. Chem.* **1976**, *120*, 1; b) A. Appel, F. Jäkle, T. Priermeier, R. Schmid, M. Wagner, *Organometallics* **1996**, *15*, 1188; c) L. Kaufmann, H. Vitze, M. Bolte, H.-W. Lerner, M. Wagner, *Organometallics* **2008**, *27*, 6215; d) B. Wrackmeyer, U. Dörfler, W. Milius, M. Herberhold, *Polyhedron* **1995**, *14*, 1425; e) A. Appel, H. Nöth, M. Schmidt, *Chem. Ber.* **1995**, *128*, 621; f) M. Scheibitz, M. Bolte, J. W. Bats, H.-W. Lerner, J. Nowik, R. H. Herber, A. Krapp, M. Lein, M. C. Holthausen, M. Wagner, *Chem. Eur. J.* **2005**, *11*, 584; g) S. Bontemps, G. Bouhadir, K. Miqueu, D. Bourissou, *J. Am. Chem. Soc.* **2006**, *128*, 12056.

[13] a) G. E. Herberich, B. Buller, B. Hessner, W. Oschmann, *J. Organomet. Chem.* **1980**, *195*, 253; b) C.-W. So, D. Watanabe, A. Wakamiya, S. Yamaguchi, *Organometallics* **2008**, *27*, 3496.

[14] B. Wrackmeyer, U. Doerfler, M. Herberhold, *Z. Naturforsch. B* **1993**, *48*, 121.

[15] a) R. E. Dinnebier, M. Wagner, F. Peters, K. Shankland, W. I. F. David, *Z. Anorg. Allg. Chem.* **2000**, *626*, 1400; b) M. Grosche, E. Herdtweck, F. Peters, M. Wagner, *Organometallics* **1999**, *18*, 4669; c) M. Fontani, F. Peters, W. Scherer, W. Wachter, M. Wagner, P. Zanello, *Eur. J. Inorg. Chem.* **1998**, 1453.

[16] D. R. Lide, *Handbook of Chemistry and Physics*, 73rd Ed, CrC Press, London, **1992**.

Received: April 18, 2012
Published online: ■■ ▮▮, 2012

Ligand Effects

H. Braunschweig, C.-W. Chiu, D. Gamon, M. Kaupp, I. Krummenacher, T. Kupfer, R. Müller, K. Radacki* ..... ▮▮▮▮–▮▮▮▮

Synthesis, Structure, and Reactivity of Borole-Functionalized Ferrocenes

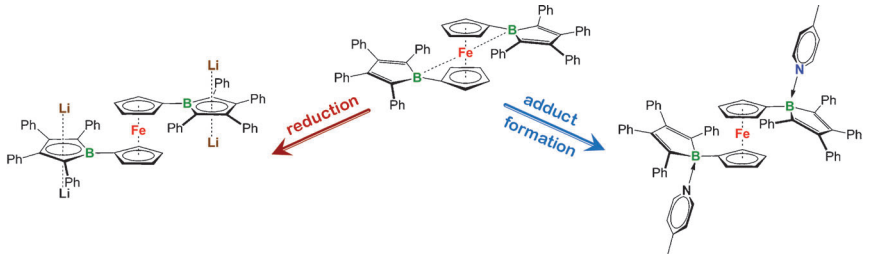

Boroles: Bisborole-functionalized ferrocene can be reduced to the corresponding tetraanion both electronically and chemically (see scheme). Compared with the previously reported monoborole-functionalized ferrocene, this compound shows a significantly enhanced Lewis acidity, which is reflected in its solid-state structure, optical properties, reduction potentials, and base-transfer reactions.

